Aalto University School of Electrical Engineering
Department of Communications and Networking

Control Channel Interference Measurement in LTE-TDD Heterogeneous Network

Guo Chen

Master Thesis submitted in partial fulfilment of the requirements for the Degree of Master of Science in Technology

Espoo, May 2015

Supervisor: Professor Olav Tirkkonen

Instructor: D.Sc Kalle Ruttik

Aalto University **Abstract of the Master's Thesis**

Author: Guo Chen

Title:
Control Channel Interference Measurement in LTE-TDD Heterogeneous Network

Date: May 2015 **Number of pages:** 61

Faculty: Electronics, Communications and Automation
Professorship: S-72 Communications Engineering

Supervisor: Professor Olav Tirkkonen

Instructor: D.Sc Kalle Ruttik

Abstract

Deploying low power eNodeBs inside macro-cells is an effective way to enhance indoor coverage. By reusing frequency between macro-cells and indoor femto-cells, the efficiency of expensive licensed spectrum can be further increased. This thesis measured Physical Downlink Control Channel (PDCCH) performance in such a heterogeneous LTE-TDD network. Four USRP software radio terminals and connected Linux workstations were deployed to build a test environment. They acted as eNodeB and UE respectively. During the test, the femto-cell was configured to coordinate its radio frame with the macro-cell. Several criteria including received block error rate, payload bit error rate and symbols signal to interference and noise ratio were used to evaluate the PDCCH performance in macro-cell under heterogeneous environment.

Keywords: PDCCH, femto-cell, heterogeneous, co-channel, eNodeB, LTE-TDD, block error rate, aggregation level

Acknowledgement

This thesis is carried out as part of the work in End-to-End Cognitive Radio Testbed (EECRT) project of Department of Communications and Networking, Aalto University.

At the beginning, I would like to express my thanks to my supervisor, Prof. Olav Tirkkonen, for his guidance of this thesis and offering me the opportunity to work in this project. Furthermore, I wish to express my great gratitude to my instructor, D.Sc. Kalle Ruttik, for providing me lots of valuable advice and comments both in the thesis as well as my RA works in the department. Thanks to their help I can finally finish this thesis. This precious experience will benefit me for a long time.

In addition, I would also like to thank Nicolas Malm, Yihenew Beyene and Jussi Kerttula for the help they gave when we worked together in this project.

At last, thanks to my family and all the friends that support and encourage me during this time.

Stockholm, 08 May 2015

Guo Chen

Contents

List of Abbreviations

BER	Bit Error Rate
BLER	Block Error Rate
BS	Base Station
CCE	Control Channel Element
CDF	Cumulative Distribution Function
CFI	Control Format Indicator
CP	Cyclic Prefix
CQI	Channel Quality Indication
CRC	Cyclic Redundancy Check
CRS	Cell-specific Reference Symbol
CSG	Closed Subscriber Group
DCI	Downlink Control Information
DL	Downlink
DMRS	Demodulation Reference Signal in PUSCH
FDD	Frequency Division Duplex
FDM	Frequency Division Multiplexing
FFT	Fast Fourier transform
GPP	General Purpose Processor

IFFT	Inverse fast Fourier transform
ISP	Internet Service Provider
LTE	Long Term Evolution
MBSFN	Multicast Broadcast Single Frequency Network
MIMO	Multiple Input Multiple Output
MUE	Macro-cell User Equipment
OFDM	Orthogonal Frequency Division Multiplexing
PBCH	Physical Broadcast Channel
PCFICH	Physical Control Format Indicator Channel
PDCCH	Physical Downlink Control Channel
PDSCH	Physical Downlink Shared Channel
PHICH	Physical Hybrid-ARQ Indicator Channel
PSS	Primary Synchronization Signal
PUCCH	Physical Uplink Control Channel
PUSCH	Physical Uplink Shared Channel
RB	Resource Block
RE	Resource Element
REG	Resource Element Group
RNTI	Radio Network Temporary Identifier
RSRP	Reference Signal Received Power
SC-FDMA	Single Carrier-Frequency Division Multiple Access
SIMO	Single Input Multiple Output
SINR	Signal to Interference plus Noise Ratio
SSS	Secondary Synchronization Signal

TDD	Time Division Duplex
TPC	Transmit Power Control
UE	User Equipment
UL	Uplink
USRP	Universal Software Radio Peripheral
3GPP	The 3rd Generation Partnership Project

List of Notations

$g_{CRC16}(D)$	Cyclic generator polynomial for 16-bit Cyclic Redundancy Check
N_{RB}^{DL}	Downlink bandwidth configuration, expressed in multiples of N_{sc}^{RB}
N_{RB}^{UL}	Uplink bandwidth configuration, expressed in multiples of N_{sc}^{RB}
N_{sc}^{RB}	Resource block size in the frequency domain, expressed as a number of subcarriers
N_{symb}^{DL}	Number of OFDM symbols in a Downlink slot
N_{ID}^{cell}	Physical layer cell identity
n_{PHICH}^{group}	PHICH group index
n_{PHICH}^{seq}	PHICH Orthogonal sequence index

List of Figures

List of Tables

Chapter 1

Introduction

The next generation cellular system is aiming to support massive number of users with simultaneous access, as well as to provide extremely high data rates within the coverage area. The way to expand system capacity or increase spectrum efficiency is the key challenges for the new system. Methods like Carrier Aggregation [1] are introduced in 3GPP LTE Release-10 for expanding the total bandwidth in usage. Up to 100MHz bandwidth can be aggregated from several component carriers [2]. However, considering the cost of purchasing licensed frequency spectrum and disposing several antennas for individual carriers, physically expanding bandwidth still has its limitation in providing high capacity efficiently. Moreover, for a normal homogeneous network contains only macro-cell, it is hard to expand the number of base stations (BS) and antennas in urban areas due to the difficulty in acquisition of appropriate sites [3].

A survey in [4] reveals that more than half of voice calls and data transmission happens in an indoor scenario. An improved deployment topology is needed for fulfilling this kind of requirement. Placing femto-cells in buildings inside macro-cells will be an effective way to provide high capacity indoor coverage. It can also solve coverage hole problems due to penetration loss of the radio link from conventional macro-cell BS to indoor User Equipment (UE) – radio signals are attenuated in the walls of the buildings. The femto-cell will use short range and low power BS, i.e. HeNodeB.

The overlaid femto-cells and macro-cells compose a Heterogeneous Network. In such a network, the co-existing femto-cells and macro-cells form a multi-tier architecture. Macro-cell BSs serve outdoor connections. Meanwhile, femto-cell BSs are deployed inside the macro-cell coverage area, serving indoor users. The penetration loss also mitigates the indoor-to-outdoor interference. Not only benefiting the indoor connection data rate, by offloading part of traffic burden from outdoor BS, the heterogeneous structure can also ensure more radio resources to outdoor connections, thereby boosting the whole network performance.

Furthermore, spatial reuse of the same frequency between indoor and outdoor, or take a so-called “co-channel” deployment, will lead to an efficient approach for capacity enhancement [5].

However, a major drawback of heterogeneous networks is inter-cell interference [6], which can lead to significant performance loss. Interference avoidance requires sophisticated interference management between femto-cell and macro-cell. Besides, a femto-cell usually serves only a predefined set of users, which locate within its coverage area. They are maintained in a list called closed subscriber group (CSG). Users outside the group are refused access to the femto-cell BS, even if they are closer to it rather than to macro-cell BS. Users not allowed to connect to femto-cell are more vulnerable to the inter-cell interference. Another detrimental aspect is the indirect connection between femto-cell BS and operator’s core network, which is usually via user’s broadband link. It limits the backhaul signaling quantity and reliability for interference coordination [7].

1.1 Scope of the thesis

Research on heterogeneous networks has paid much attention to interference coordination between macro-cells and femto-cells. In heterogeneous networks with co-channel deployment, interferences can be divided into control channels interference and data channel interference. LTE control channels carry connection signaling and resource grant information. They only occupy a small part of the radio resource but are vital for establishing the data connection. From a system operation point of view, it is critical to have good reception quality of control channels. Failure in decoding control signaling will also disable the access of data channels. Physical Downlink Control Channel (PDCCH) is the most important control channel in LTE. It carries the Downlink Control Information (DCI) as payload and is convolutionally encoded. Convolutional codes are weaker than turbo codes that are used by data channels. Hence, identifying how well the PDCCH can sustain the inter-cell interference in a heterogeneous network is crucial.

The reliance of control channel performance against interference in the heterogeneous network is usually studied with simulations or with theoretical modeling. In this thesis, we measure how inter-cell interference impacts the PDCCH performance in a realistic environment that is built by using Universal Software Radio Peripheral (USRP) frontends.

The USRP shifts signals to and from radio frequencies. The baseband functionalities are implemented in Linux workstations by software. Such software defined radio (SDR) platform provides flexible and configurable radio test environment. In our test, one USRP and one connected Linux workstation compose a basic node, performs functionalities of an LTE BS

(eNodeB) or a UE. Several nodes are deployed at the same time to form the heterogeneous network environment.

In a heterogeneous network, macro-cell UEs are more vulnerable to the inter-cell interference in some circumstances, compared to femto-cell UEs. For example, when a macro-cell UE moves indoor or stays much closer to the HeNodeB than the macro-cell eNodeB, it will receive strong interference from femto-cell while being served by a distant macro-cell eNodeB. It may severely worsen macro-cell UE user experience. Therefore, it is very interesting to focus on the potential macro-cell PDCCH performance degradation brought by inter-cell interference in a heterogeneous network.

In the thesis, the macro-cell PDCCH reception quality at the macro-cell UE will be measured under different inter-cell interference levels. The PDCCH block error rate (BLER) and payload bit error rate (BER) will be used as criteria to reveal the relation between PDCCH performance and co-channel inter-cell interference.

1.2 Thesis Organization

The thesis starts with the brief explanation of LTE heterogeneous network and reviews the recent research on inter-cell interference management methods. Chapter 3 explains how OFDM is used in LTE Downlink transmission. In Chapter 4, LTE-TDD physical layer concepts are described. The physical layer channels structures and mappings are introduced in Chapter 5. Chapter 6 interprets the Downlink physical layer channels decoding methods and procedures. Chapter 7 gives the implementation of a USRP based heterogeneous network test environment. Followed by Chapter 8, it presents the measurement results on PDCCH in the heterogeneous network and corresponding analysis. An improved model is also proposed for conducting future measurement. At last, Chapter 9 is the overview and conclusion of the whole thesis.

Chapter 2

Model of LTE Heterogeneous Network

2.1 Femto-Cell Structure

The explosive smart devices market in recent years generates huge demand for wireless data services. For mobile network operators, the conventional way of offering more capacity and enhancing coverage is to deploy more BSs, purchasing more licensed frequency spectrum and adopting methods to increase spectrum efficiency. CISCO indicates in [8] that around 80% mobile data traffic happens indoor according to its network analytics. However, indoor environment brings great challenges on signal coverage. The building walls and obstacles inside buildings attenuate or block the signal propagation. The higher carrier frequencies used in 4G is more vulnerable to such penetration loss than the lower frequencies used in old generation standards. The indoor coverage and data throughput as a consequence will decline.

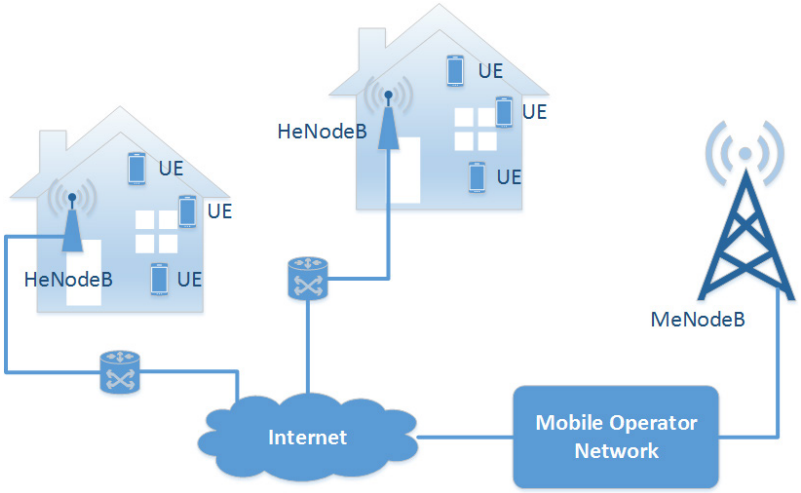

Figure 2.1: Connection of typical femto-cell and macro-cell to the operator core network

A cost-effective solution to improve indoor user experience is to deploy small range indoor BSs. The LTE femto-cell is a small BS with low transmission power and short cover

range. Figure 2.1 displays a typical structure of femto-cell network. As a complement to operator's macro-cell network, femto-cell BSs are typically installed indoors. They offer coverage enhancement, throughput escalation, traffic offloading, and even location-based services [9]. An LTE femto-cell BS is sometimes called HeNodeB, as a shorthand for Home eNodeB. Comparably, MeNodeB stands for regular macro-cell eNodeB. HeNodeB and MeNodeB provide the same air interface. UE can access either HeNodeB or MeNodeB without modification of signaling. The HeNodeB is connected to the mobile operator's core network through wired broadband link such as DSL or fiber.

The HeNodeBs can be configured into two modes, either Closed Subscriber Group (CSG) or Open Subscriber Group (OSG). With CSG, each HeNodeB will maintain a list of subscribers who can be connected to it. The 3GPP specifications define CSG options for LTE networks. In OSG configuration, HeNodeBs are open to all UEs.

2.2 Femto-Cell and Macro-Cell Overlaid Heterogeneous Network

A heterogeneous network is a network where there is a tier of macro cells, and in addition, one or more tiers of small cells deployed in the macro tier coverage area. Here we consider a situation where the small cells are femto-cells.

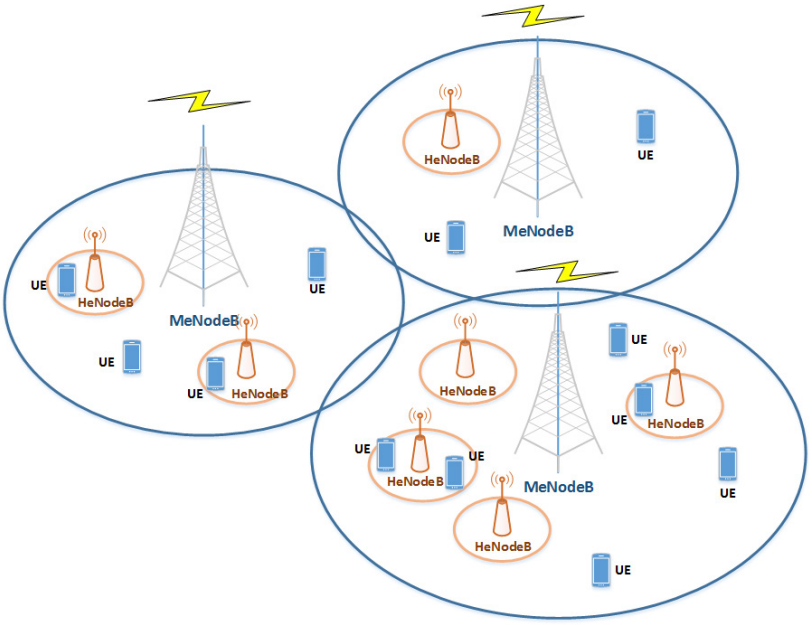

Figure 2.2: An example structure of LTE heterogeneous network

A heterogeneous network example is illustrated in Figure 2.2. In such a configuration macro-cell eNodeBs belong to a Tier-1 network and femto-cell HeNodeBs belong to a Tier-2 network. Tier-1 network provides wide area coverage and serves large quantities of macro-cell UEs while tier-2 network serves indoor CSG users. One of the challenges that a heterogeneous network faces is the radio resource management between femto-cells and macro-cells. One could envision three interference management methods: exclusive frequency allocation, overlapping frequency allocation and partially overlapping frequency allocation, shown in Figure 2.3. Usually, radio frequency is used orthogonally, macro-cell and femto-cell each has an exclusive part. That, however, reduces the available capacity. It is more efficient to use whole spectrum in both macro-cell and femto-cells. If macro-cell and femto-cell use the same frequencies, they have to deal with the generated interference. The interference has to be maintained such that QoS target in all the cells remain within acceptable level. The inter-cell interference management and coordination are especially important for users at cell edge or overlapped area [10].

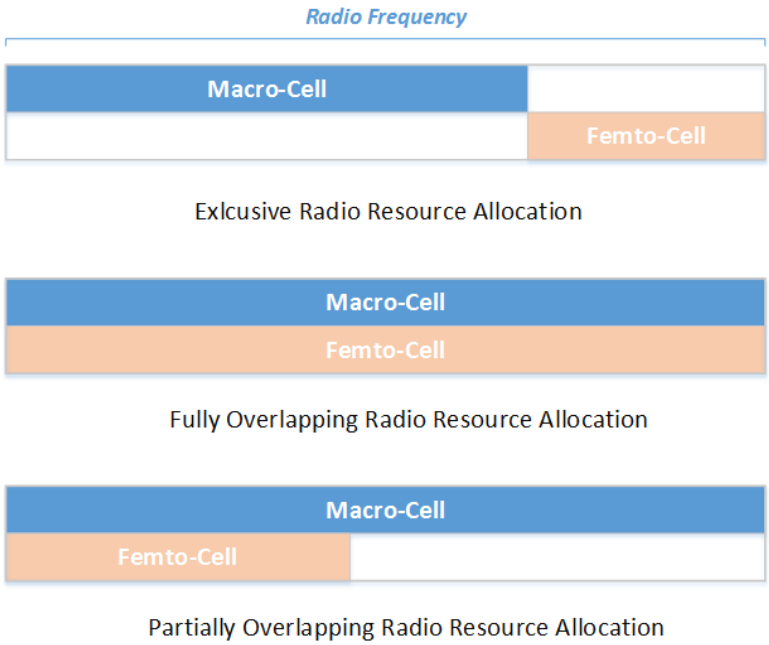

Figure 2.3: Radio resource share scheme between femto-cell and macro-cell

In exclusive radio resource allocation method, macro-cell and femto-cell are each allocated with their own radio resource blocks. No cross-tier interference will happen since femto-cell and macro-cell spectrums are not overlapped. The spectrum efficiency is achieved by utilization of different load characteristics in macro-cell and femto-cell. The peak demand for femto-cell is usually during the day time while macro-cell needs more resources during users commuting i.e. rush hours. Dynamically adjustable radio resource allocation should be achieved for increasing the spectrum efficiency. Usually, macro-cell is the primary user of spectrum with higher privilege, while the secondary user, femto-cell will be required to

possess the capability of spectrum sensing, for identifying free resource blocks and avoiding the overlap with primary user's data transmission. Femto cell eNodeB can use techniques like energy detection, waveform-based sensing, matched filtering, etc to implement spectrum sensing. However the limitation is bad performance under low SINR environment or increased system complexity [11][12][13][14].

In spectrum overlay approach, femto-cell eNodeB will be granted part of or whole spectrum used by macro-cell eNodeB. Since both cells are using the same spectrum, some type of interference coordination is required. Usually the macro-cell is the primary spectrum user and the femto-cell eNodeB needs to adjust its transmission according to the macro-cell eNodeB requirements. This scenario would benefit from interference cancellation algorithm, implemented in UE or eNodeB.

2.3 Recent Research on Femto-Cell Overlaid Heterogeneous Network

One of the major concerns of heterogeneous network is effective approaches to mitigate femto-cell to macro-cell interference. The macro-cell UEs that are also in femto-cell coverage area receive signals from both HeNodeB and MeNodeB. One of those could interfere the other's signal.

LTE subframe contains multiple OFDM (Orthogonal Frequency Division Multiplexing) symbols. Into those symbols are multiplexed bits corresponding to control and data channels. Control channels are located into first 1-3 OFDM symbols. In [15], a method taking advantage of control region sparseness is introduced. In macro-cell, eNodeB needs to serve a large quantity of UEs. As a result, a lot of control channel capacity is needed. Therefore, more than one OFDM symbols will be configured for control channels. In femto-cell, eNodeB usually serves very few users. The need for control signaling is much less and only fewer OFDM symbols are sufficient for serving the requirement.

Since OFDM symbols for data region come after control region symbols, in case only configuring single OFDM symbol as control region in femto-cell, the adjacent data region of it will cast overlapping onto the macro-cell control region. Hence, the improvement of macro-cell control channel performance could be achieved by avoid overlapping comes from femto-cell data region. Femto-cell eNodeB will be enforced to utilize same size of OFDM symbols for control region as macro-cell eNodeB does, regardless of actual payload requirement. Femto-cell eNodeB can spread PDCCHs over the whole control region, leaving a lot of spare UEs as shown in Figure 2.4. This method is simple, does not add any additional

signaling or require extensive computation. However, it brings capacity loss in femto-cell since a lot of spare UEs are wasted.

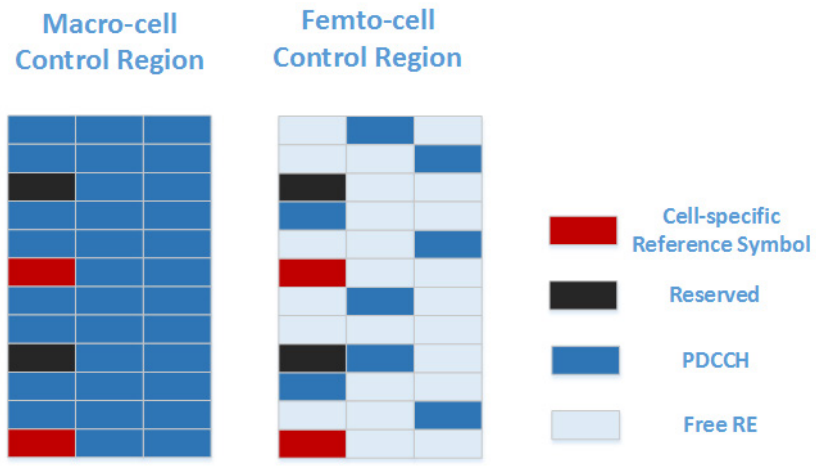

Figure 2.4: Femto-cell control region sparseness for interference control

A similar mechanism is to insert Almost Blank Subframe (ABS) between normal subframes during transmission [15][16][17]. The concept of ABS is displayed in Figure 2.5. Femto-cell eNodeB should be muted in ABS. In these subframes it is only allowed to transmit Cell-specific Reference Symbols (CRS), and if required, Primary Synchronization Signal (PSS), Secondary Synchronization Signal (SSS) and Physical Broadcast Channel (PBCH). The Almost Blank Subframe reduces the interference. Unfortunately, ABS method requires time synchronization of radio frames between macro-cell and femto-cell and that increases system complexity.

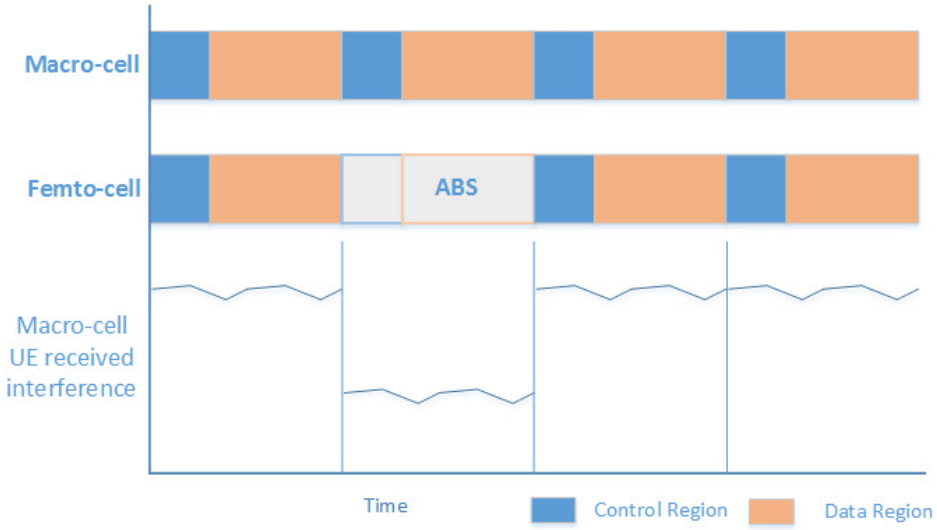

Figure 2.5: Using Almost Blank Subframe (ABS) to mitigate femto-cell to macro-cell interference

Femto-cell eNodeB transmit power control [15][18] is another approach of control channel interference deduction. Femto-cell eNodeB will adjust its transmission power according to mean of the Reference Signal Received Power (RSRP) of the strongest macro-cell, i.e. $\overline{R_{CRS}}$. The HeNodeB transmit power will be reduced when received $\overline{R_{CRS}}$ is low. However, since transmission power is reduced, femto-cell transmission capacity and coverage area will be reduced as well.

A macro-cell control channel protection algorithm that uses physical layer cell ID manipulation is presented in [19]. In the LTE subframe, Cell-specific Reference Symbol (CRS), Physical Control Format Indicator Channel (PCFICH) and Physical Hybrid-ARQ Indicator Channel (PHICH) positions depend on the cell ID. By changing own cell ID to be different than the macro-cell ID, femto-cell HeNodeB can avoid overlap of its own CRS, PCFICH and PHICH with corresponding macro-cell channels. HeNodeB can sense macro-cell ID by detecting its PSS and SSS [20]. However, the overlapping of PDCCH may still happen, as its position is independent with cell ID.

Chapter 3

Downlink OFDM Transmission in LTE

OFDM, Orthogonal Frequency Division Multiplexing, is utilized in LTE Downlink radio transmission, regarding overcoming frequency selective fading issue while providing high spectrum efficiency. OFDM scheme will convert a group of high data rate serial signals into low data rate parallel signals. After being mapping into resource grid, physical layer complex-valued symbols will be transformed into OFDM symbols. A set of narrow band subcarriers, which are mutually orthogonal, will be employed to carry these parallel signals. Each subcarrier is corresponding to one modulated complex-valued symbol.

This chapter will briefly introduce the principle of OFDM as well as the OFDM encoder and decoder used in LTE radio transmission.

3.1 Principle of OFDM

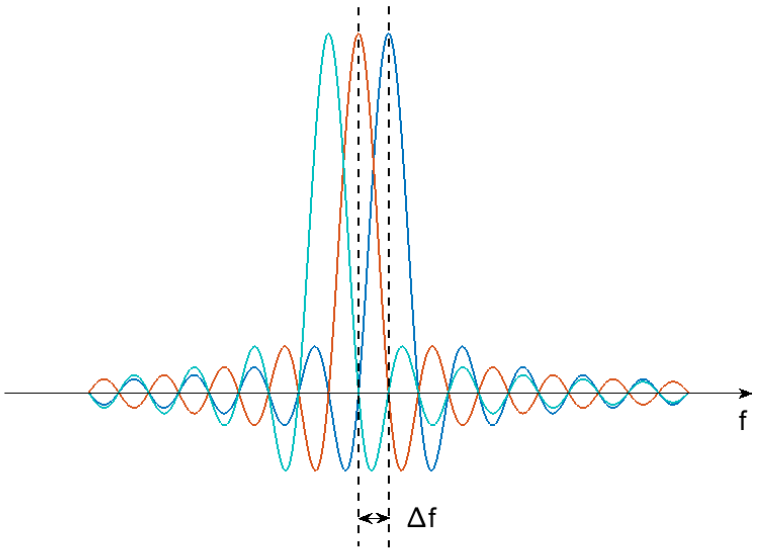

Figure 3.1: Spectrum of OFDM subcarriers

Unlike a conventional frequency division multiplexing (FDM) scheme, in which the subcarriers are isolated in frequency domain, OFDM allows its subcarriers to overlap with each other. The Figure 3.1 shows the spectrum of OFDM system. The orthogonality ensures the peak of each subcarrier locates at the zero-crossing point of adjacent subcarriers. Therefore, if precisely sampled at central frequency, all the subcarriers will not interfere with each other.

The principle of a typical OFDM transmission system is described in Figure 3.2. The OFDM encoder has N individual modulators. A stream of serial complex-valued symbols, $(a_0, a_1, \dots, a_{N-1})$ are sent into encoder, becoming parallel. Symbols are modulated to different subcarriers with frequencies of $f_0, f_1, \dots, f_{N-1}$ respectively. The frequency interval of adjacent subcarriers is $\Delta f = 1/T$. In LTE system, $\Delta f = 15kHz$.

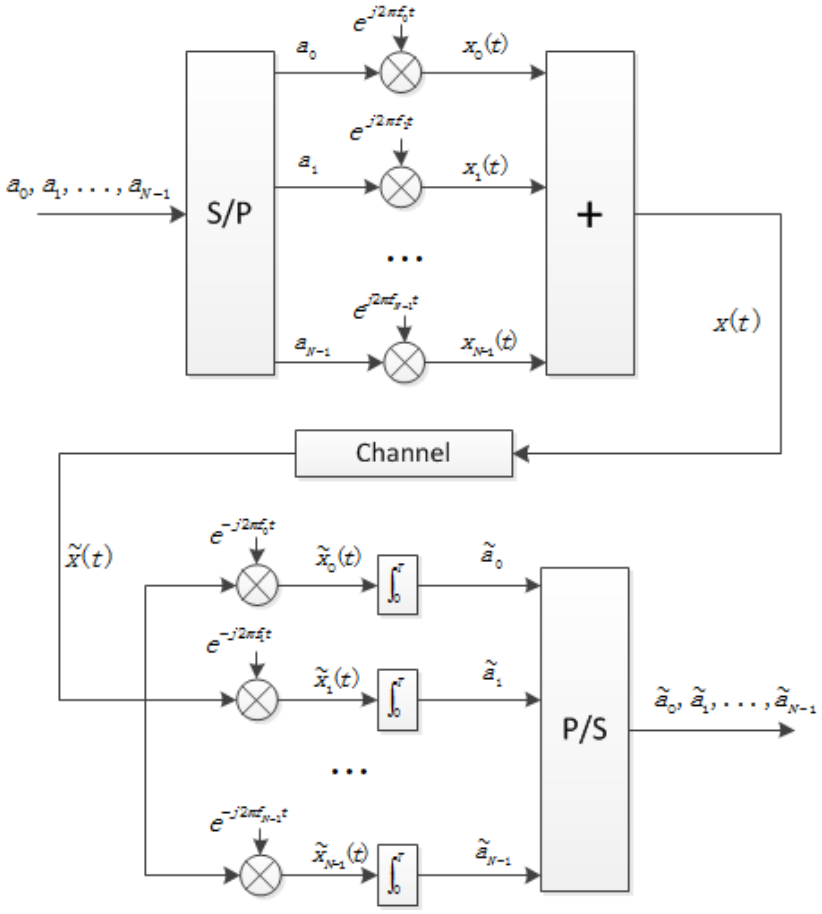

Figure 3.2: A typical OFDM modulation and demodulation system

The frequency domain OFDM encoder output signal can be expressed as:

$$X(f) = \sum_{k=0}^{N-1} a_k * X_c(f - k * \Delta f)$$

Within which, $X_c(f)$ is the subcarrier expression in frequency domain. The corresponding time domain OFDM signal in an interval of $[-T/2, T/2]$ will be:

$$x(t) = \frac{1}{T}\sum_{k=0}^{N-1} a_k * e^{j2\pi k\Delta f t} = \frac{1}{T}\sum_{k=0}^{N-1} a_k * e^{j\frac{2\pi k}{T}t} \qquad t \in [-T/2, T/2]$$

Thanks to the orthogonality of subcarriers, OFDM decoder can split each symbol by calculation integral of received subcarrier on $t \in [-T/2, T/2]$.

$$\frac{1}{T}\int_{-\frac{T}{2}}^{\frac{T}{2}} x_{m1}(t) * x_{m2}(t)\, dt = \frac{1}{T}\int_{-\frac{T}{2}}^{\frac{T}{2}} a_1 a_2 * e^{j\frac{2\pi k_1}{T}t} * e^{-j\frac{2\pi k_2}{T}t} dt$$

$$= \frac{1}{T}\int_{-\frac{T}{2}}^{\frac{T}{2}} a_1 a_2 * e^{j\frac{2\pi(k_1-k_2)}{T}t} dt = \begin{cases} 0 & k_1 \neq k_2 \\ a_1 a_2 & k_1 = k_2 \end{cases}$$

Hence, for a complex-valued symbol a_k, it can be recovered as below:

$$\int_{-\frac{T}{2}}^{\frac{T}{2}} \tilde{x}_m(t)\, dt = \int_{-\frac{T}{2}}^{\frac{T}{2}} \frac{1}{T}\sum_{k=0}^{N-1} \tilde{a}_k * e^{j\frac{2\pi k}{T}t} * e^{-j\frac{2\pi m}{T}t} dt$$

$$= \frac{1}{T}\int_{-\frac{T}{2}}^{\frac{T}{2}} \sum_{k\neq m} \tilde{a}_k * e^{j\frac{2\pi k}{T}t} * e^{-j\frac{2\pi m}{T}t} dt + \frac{1}{T}\int_{-\frac{T}{2}}^{\frac{T}{2}} \tilde{a}_k dt$$

$$= 0 + \tilde{a}_k = \tilde{a}_k$$

In continuous signal system transmitter side, it needs to generate a number of N different subcarriers with Δf frequency. On the receiver side, it also needs N different subcarriers and doing N times integral in order to recover out all the signals.

3.2 OFDM Encoding and Decoding in LTE

Unlike continuous signal processing principle showed above, the real LTE system use time discrete OFDM signals. N-Point IFFT (Inverse Fast Fourier Transform) is used as OFDM encoder and N-Point FFT (Fast Fourier Transform) is used as OFDM decoder, explained in Figure 3.3 and Figure 3.4.

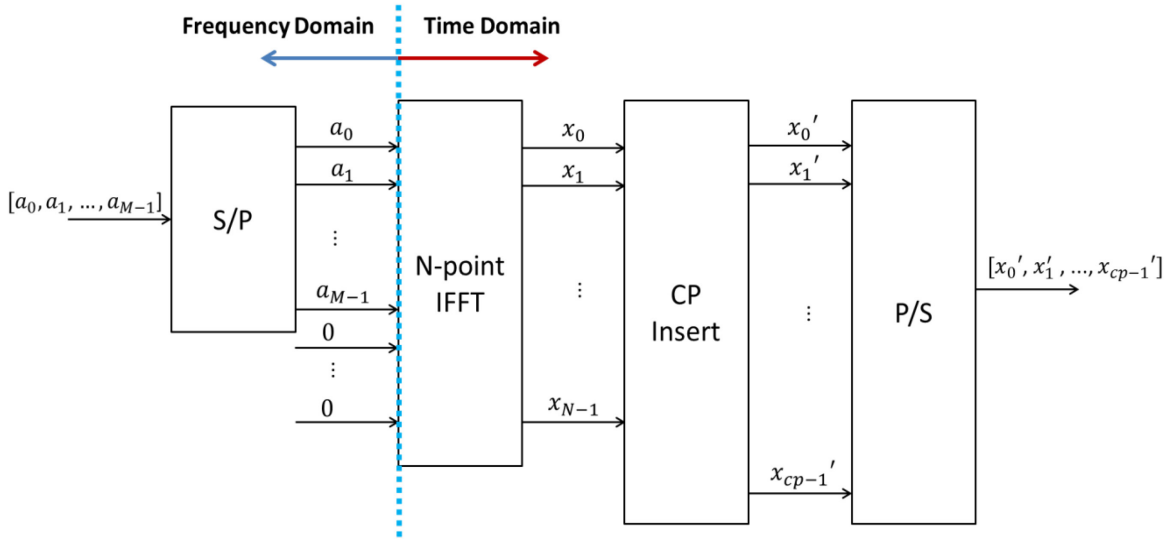

Figure 3.3: OFDM encoder with cyclic prefix

The transmitter does not need to modulate each route signal individually. The IFFT module works in frequency domain, directly calculates out the time domain summation of N routes orthogonal signal. On the other hand, the receiver no longer needs to do integral as FFT will directly recover back the frequency domain signal of each orthogonal route.

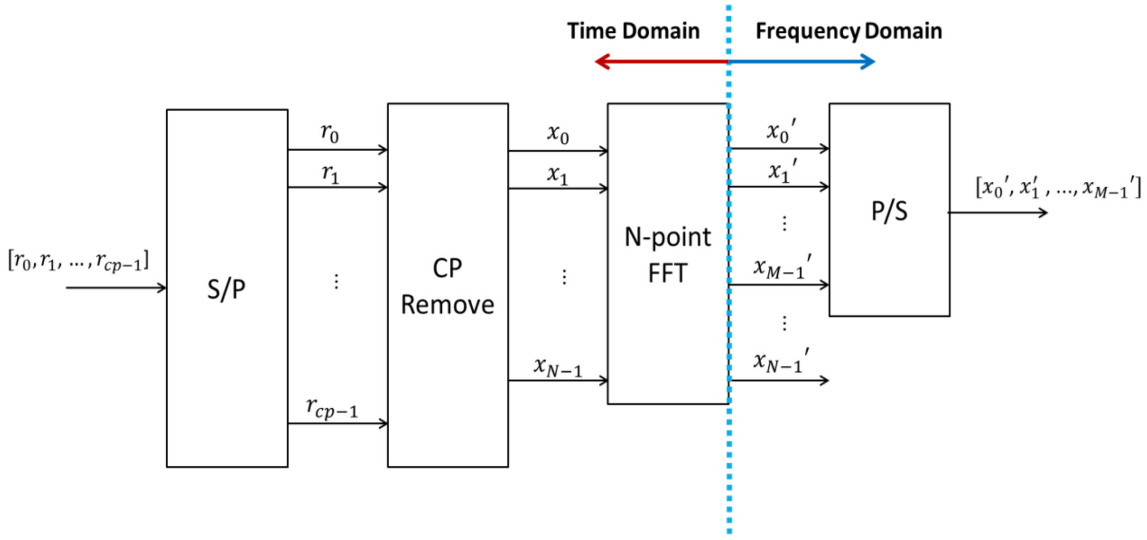

Figure 3.4: OFDM decoder with cyclic prefix

M complex-valued symbols are sent to the encoder. Several zeroes need to be inserted after serial-to-parallel transforming, for fulfilling the IFFT size N.

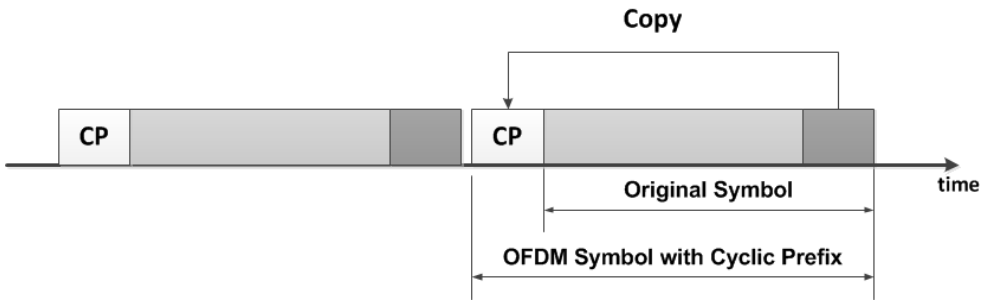

Figure 3.5: Cyclic Prefix concept

In order to provide robustness against Inter Symbol Interference caused by multipath distortion, Cyclic Prefix (CP) is also introduced. A cyclic prefix insertion module is deployed after N-Point IFFT. It works in time domain, copying last section of OFDM symbol into its beginning, as displayed in Figure 3.5. Correspondingly, the cyclic prefix needs removal at receiver side before conducting FFT. As long as the delay of the reception symbol is not bigger than the time length of CP, the receiver can correctly recover the symbol.

Chapter 4

LTE Physical Layer Concepts

In this section, we describe LTE physical layer structure, frame definition and basic resource units. We also discuss the advantages and disadvantages between LTE-TDD mode and LTE-FDD mode as well as why we are interested in choosing TDD mode in our system implementation.

4.1 LTE Physical Frame Structure

According to 3GPP LTE technical specifications release 8, both Downlink and Uplink signal transmission of LTE radio signal is confined into 10 ms frames [21]. Each radio frame consists of ten 1ms subframes. One subframe is divided into two 0.5 ms slots. The specification defines two types of radio frame structure, Type 1, which is applicable for LTE-FDD system, while Type 2 is applicable for LTE-TDD system.

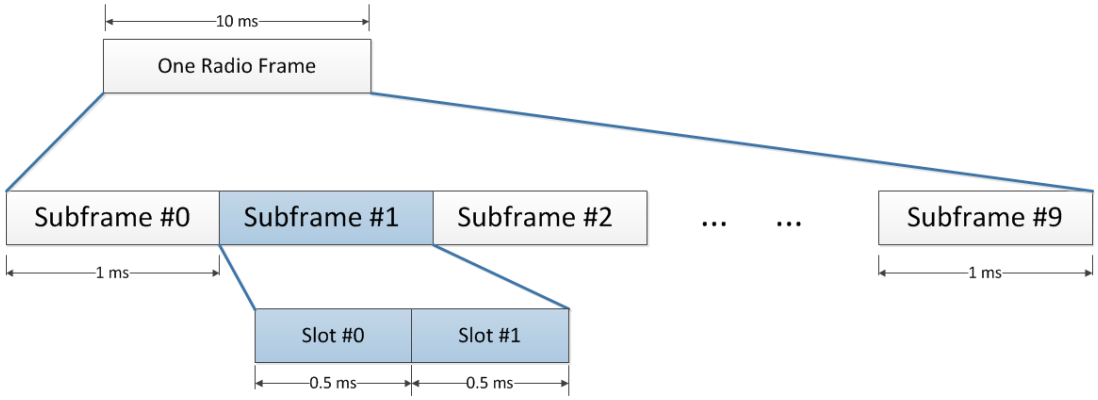

Figure 4.1: LTE radio frame structure

Regardless of physical layer frame structure difference, TDD mode and FDD mode have similar higher layers operation procedures [22]. However, the TDD mode has some advantages compared to the FDD mode [23][24][25][26].

Since Uplink (UL) and Downlink (DL) transmission are duplexed in the same frequency, TDD mode does not require paired spectrum for UL and DL individually. The expense of purchasing the licensed TDD band is usually lower compared to the FDD band. Besides, implementation of TDD devices is also less expensive consider as they require less expensive RF components (e.g. no RF frequency duplex filter is needed). In addition, TDD mode is more suitable for MIMO implementation. The quality of MIMO highly depends on the accurate channel estimation. In TDD mode, the measured channel characteristics of UL can be used for DL as well after precise calibration. The implementation of MIMO in FDD mode is comparably more difficult.

TDD mode also supports asymmetric DL/UL resource allocation. The 3GPP LTE technical specifications define seven Uplink-Downlink configurations [21]. Each subframe can be reserved for Downlink transmission (represented as “D”), Uplink transmission (represented as “U”) or it may be a special subframe (“represented as “S”). The configurations are listed in Table 4.1. These different configurations in TDD mode provide more flexibility to fulfill various capacity requirement patterns between DL and UL.

Table 4.1: LTE-TDD Uplink-Downlink configurations [21]

Uplink-Downlink configuration	Subframe number									
	0	1	2	3	4	5	6	7	8	9
0	D	S	U	U	U	D	S	U	U	U
1	D	S	U	U	D	D	S	U	U	D
2	D	S	U	D	D	D	S	U	D	D
3	D	S	U	U	U	D	D	D	D	D
4	D	S	U	U	D	D	D	D	D	D
5	D	S	U	D	D	D	D	D	D	D
6	D	S	U	U	U	D	S	U	U	D

On the other perspective, TDD mode also brings some disadvantages [23][24][25][27].

TDD mode requires UL/DL configuration type and switching time coordination between cells in order to avoid time duplexing interference. A UE that is transmitting at the high power level will severely interfere another UE nearby which is receiving a weak signal from a distant eNodeB. In addition, due to the discontinuous transmission, coverage of a TDD eNodeB is also smaller than an FDD eNodeB in case they use same power level.

Besides, the guard period for DL/UL switch in special subframes leads to resource waste since no data can be transmitted during that time. Moreover, TDD mode has latency issue. The acknowledgement of DL reception needs to wait until following UL subframes before it can be transmitted. The situation will become even worse when UL subframes number is

very small in asymmetric UL/DL configurations, i.e. configuration 5 in which only one UL subframe exists per every 8 DL subframes.

In the real commercial environment, operators usually need to make a compromise and consider the above characteristics when choosing their LTE system duplex mode.

However, when it comes to our heterogeneous network scenario that contains indoor small cells, some features make LTE-TDD mode more interested to us. The small size of indoor femto-cell is not sensitive to the TDD coverage issue. The low cost of TDD eNodeB will also be attractive to the users. TDD's advance on MIMO deploying benefits the indoor high throughput requirement. Moreover, some shortages of TDD mode become less harmful [23]. The time duplexing interference between indoor femto-cell and ourdoor macro-cell can be mitigated by building wall isolation.

In this thesis we will use LTE-TDD standard to implement our system and conduct the measurement. Hence, in the below introduction of LTE physical layer concept we will discuss only Type 2 LTE-TDD structure and denote it as the default.

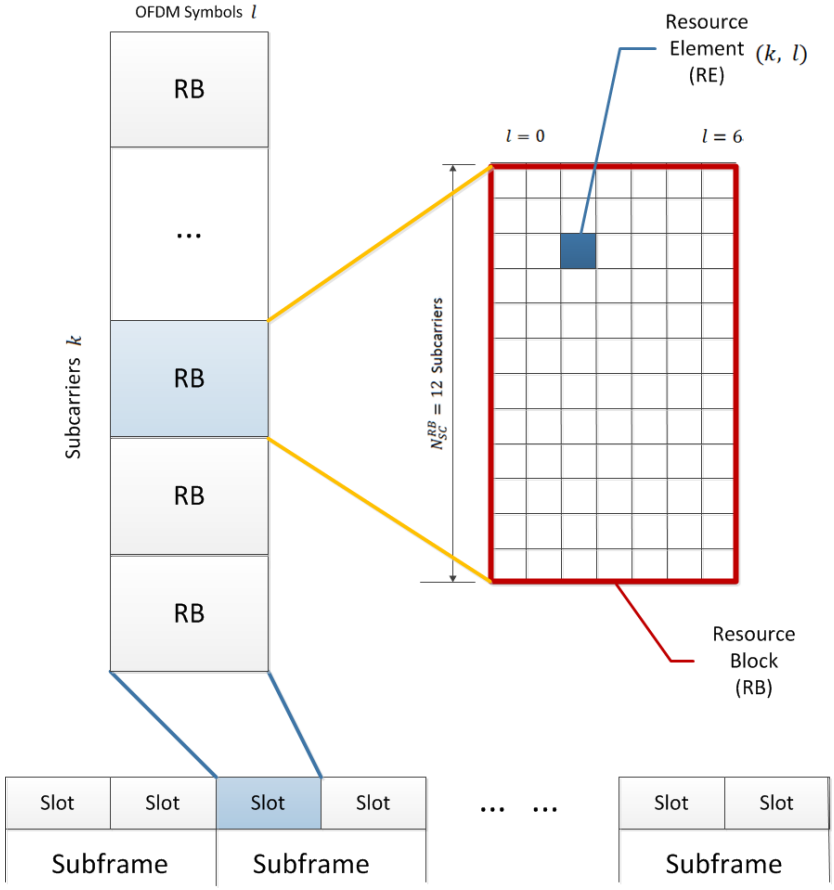

Figure 4.2: LTE-TDD Downlink subframe resource grid

The transmitted radio signal within each slot is mapped to time-frequency resource grid, shown in Figure 4.2. The resource grid contains OFDM symbols in DL, or SC-FDMA symbols in UL.

The basic time-frequency unit in the grid is call Resource Element, or RE. One 0.5 ms slot contains seven symbols. One RE is one subcarrier by one symbol. The distance between adjacent subcarriers is 15 kHz, i.e. frequency distance between two consecutive REs is 15 kHz. Each RE in the grid can be identified as index pair (k, l), within which k is frequency domain indices and l is time domain indices.

In order to describe the mapping of modulated physical signal symbols into the resource elements, REs are grouped into resource blocks (RB). One resource block contains twelve consecutive subcarriers in frequency domain, and seven consecutive symbols in a slot, respectively. RB is used as a unit to describe transmission bandwidth of DL and UL. For both DL and UL, the current specification indicates the smallest transmission bandwidth to be 6RBs, occupying 1.08 MHz in frequency. While the largest to be 100RBs, occupying 18 MHz in frequency [28].

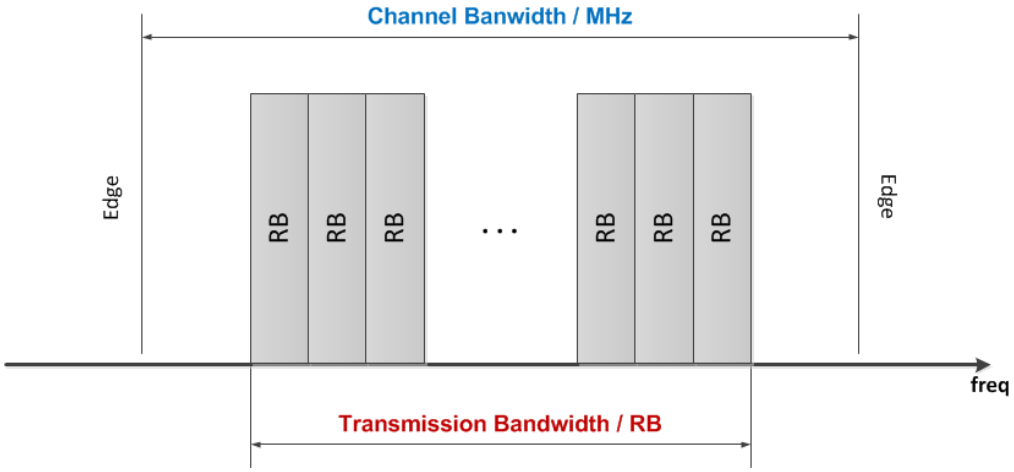

Figure 4.3: Relation between LTE channel bandwidth and transmission bandwidth.

It should be reminded that transmission bandwidth is different for different channel bandwidths. As displayed in Figure 4.3, the transmission bandwidth is usually smaller than the channel bandwidth. The idea is to providing the guard band between the transmissions of different operators, protecting them from adjacent channel interference.

There are six different transmission bandwidth configurations defined in LTE, listed in Table 4.2. In the rest of this thesis, DL or UL bandwidth usually refers to transmission bandwidth.

Table 4.2: LTE transmission bandwidth configurations

Channel BW (MHz)	Transmission BW (RB)	Occupied BW (MHz)
1.4	6	1.08
3	15	2.7
5	25	4.5
10	50	9
15	75	13.5
20	100	18

4.2 REG and CCE

The resource grid will be loaded with physical layer symbols, including reference symbols, synchronization symbols, control channel symbols and shared channel symbols. Depending on the usage, the LTE-TDD resource grid can be divided into two regions: control region and data region.

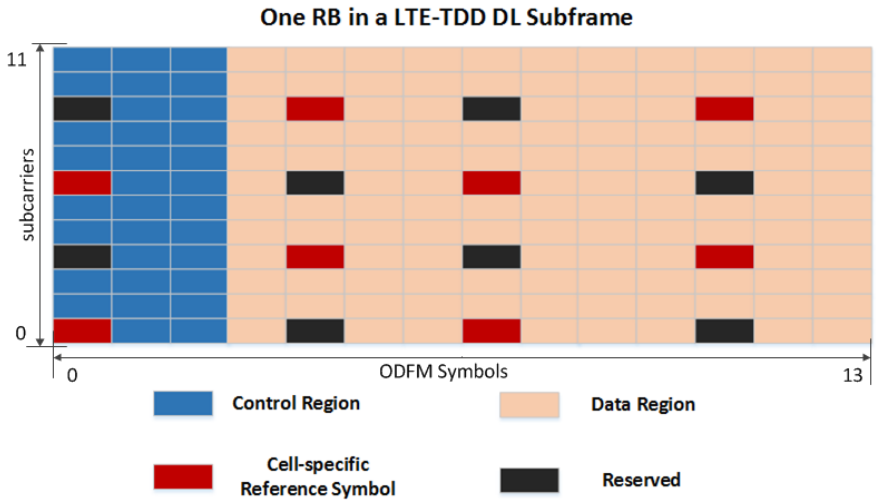

Figure 4.4: Control region and data region of a subframe

The control region, used for carrying control signaling, includes Physical Control Format Indicator Channel (PCFICH), Physical Hybrid-ARQ Indicator Channel (PHICH) and Physical Downlink Control Channel (PDCCH).

The data region is used for carrying data signal. It contains the Primary Synchronization Signal (PSS), Secondary Synchronization Signal (SSS), Physical Downlink Shared Channel (PDSCH), Physical Broadcast Channel (PBCH), etc. Cell-specific reference symbols are contained both in the control region and the date region.

In an LTE DL subframe, the control region usually occupies the first 1 to 3 OFDM symbols (for 1.44MHz channel bandwidth, it is 2 to 4 OFDM symbols, due to the limited REs number within each symbol). The exact symbols number configured depends on system bandwidth and the cell load. The rest OFDM symbols are occupied by data region.

Figure 4.4 illustrates a DL subframe where control region consists of three symbols. This figure is only for normal DL subframe. It does not consider Multimedia Broadcast Single Frequency Network (MBSFN) subframe. MBSFN subframe is used for providing Multimedia Broadcasting service. It uses a different structure than normal DL subframe. The number and locations of MBSFN depend on the network configuration.

In order to schedule the control channel resources effectively, 3GPP LTE specification defines two basic resource units, Resource Element Group (REG) and Control Channel Element (CCE), dedicatedly for control region usage.

REG represents four consecutive unused resource elements in one OFDM symbol. It could be four physically consecutive REs, or in another situation that usually happens in the first OFDM symbol of a subframe, six REs, within which two REs are used by cell-specific reference symbols. Few REGs are used for PCFICH and PHICH allocation. These two channels carry a relatively low amount of data. Compared to them, PDCCH size can be bigger. CCE, which consists of 9 unused REGs, is used as the basic unit for allocating PDCCH data.

Chapter 5

LTE DL Physical Channel Structure

This section focuses on the structure of the major DL physical layer control channels in LTE-TDD standard, including PCFICH, PHICH and PDCCH, as well as their corresponding algorithms of encoding and mapping.

5.1 PCFICH

PCFICH carries Control Format Indicator (CFI). The value of CFI ranges from 1 to 4, informs UE the size of the control region. The relation between CFI values and control region size is illustrated in Table 5.1. When Downlink bandwidth $N_{RB}^{DL} > 10$, control region symbols number equals CFI value. On the other hand, when Downlink bandwidth $N_{RB}^{DL} \leq 10$, control region symbols number equals CFI + 1. A special case is in subframe 1 and subframe 6, which have PSS symbols on 3rd OFDM symbol. In these subframes, the number of OFDM symbols scheduled for control region cannot surpass two.

Table 5.1: Number of OFDM symbols for control region

	DL Bandwidth / CFI Value	$N_{RB}^{DL} > 10$	$N_{RB}^{DL} \leq 10$
Subframe 1 and 6	1	1	2
	2	2	N/A
Other subframes	1	1	2
	2	2	3
	3	3	4

CFI value is protected by simple repetition coding. The 32-bit codewords are shown in Table 5.2. The all-zero codeword of CFI=4 is reserved and currently not used.

Table 5.2: CFI code words [21]

CFI	CFI codeword $< b_0, b_1, \dots, b_{31} >$
1	$<$ 0,1,1,0,1,1,0,1,1,0,1,1,0,1,1,0,1,1,0,1,1,0,1,1,0,1,1,0,1,1,0,1 $>$
2	$<$ 1,0,1,1,0,1,1,0,1,1,0,1,1,0,1,1,0,1,1,0,1,1,0,1,1,0,1,1,0,1,1,0 $>$
3	$<$ 1,1,0,1,1,0,1,1,0,1,1,0,1,1,0,1,1,0,1,1,0,1,1,0,1,1,0,1,1,0,1,1 $>$
4	reserved, all-0

The same CFI codewords are used in all the cells. The codewords in different cells are protected by cell-specific scrambling sequences [21]. The scrambled 32-bit codewords will be modulated using QPSK scheme, becomes 16 complex-valued symbols. In this thesis, layer mapping and precoding techniques will not be considered. The 16 complex-valued symbols are directly mapped to first OFDM symbol of each DL subframe. The mapping is done by grouping the 16 symbols into four symbol groups, expressed as $z^{(p)}(0)$, $z^{(p)}(1)$, $z^{(p)}(2)$ and $z^{(p)}(3)$, each contains four symbols. In order to obtain frequency diversity gain, four groups are mapped into four REGs. These REGs are uniformly distributed over whole transmission bandwidth, based on the rules listed below:

$z^{(p)}(i)$ is mapped to resource element group represented by index k_i,

$$k_i = \bar{k} + \left\lfloor i * N_{RB}^{DL}/2 \right\rfloor \cdot N_{sc}^{RB}/2 \qquad i = 0, 1, 2, 3$$

of which, $\bar{k} = (N_{sc}^{RB}/2) \cdot (N_{ID}^{cell} \; mod \; 2N_{RB}^{DL})$. After calculation, k_i will modulo $N_{RB}^{DL} * N_{sc}^{RB}$. N_{ID}^{cell} is physical layer cell identity number.

Figure 5.1 summarizes the PCFICH coding and mapping procedures.

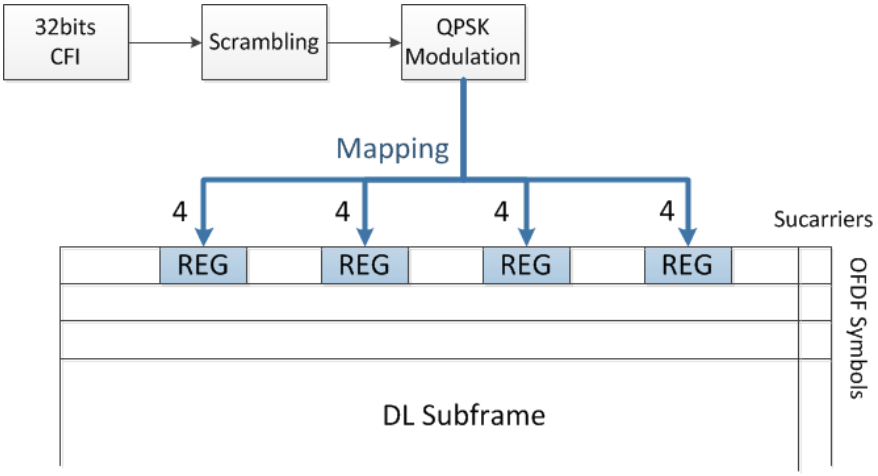

Figure 5.1: PCFICH processing procedures

5.2 PHICH

Physical Hybrid-ARQ Indicator Channel (PHICH), carries feed-back Hybrid ARQ information. After Physical Uplink Shared Channel (PUSCH) data transmission, UE waits for ACK/NACK feedback from eNodeB. This feedback is coded in PHICH. PHICH is carried in first one to three OFDM symbols in a subframe. Several PHICHs can be multiplexed into a same set of REs. These PHICHs form a PHICH-group. Several PHICH groups can exist in one subframe. The PHICH multiplexing is achieved by using orthogonal sequence.

Two parameters, PHICH-Duration and PHICH-Resource index pair, will define the PHICHs distribution and help to identify each specific one.

PHICH-Duration indicates the OFDM symbols number used by PHICHs. According to Table 6.9.3-1 in [21], in normal situation, PHICHs only occupy the first OFDM symbol. In order to provide extra time diversity gain, extended PHICH duration will be used. It will need 2 or 3 symbols regarding the subframe type. In this thesis, only the normal duration is used.

PHICH-Resource index pair is defined as $(n_{PHICH}^{group}, n_{PHICH}^{seq})$. n_{PHICH}^{group} is the PHICH group index, which is used to distinguish different PHICH groups. n_{PHICH}^{seq} is the orthogonal sequence index, is used to distinguish PHICHs within a same PHICH group.

According to PHICH specification in [21], maximum PHICH group number is defined by $m_i * N_{PHICH}^{group}$.

$$n_{PHICH}^{group} = \begin{cases} \lceil N_g \, (N_{RB}^{DL} / 8) \rceil & for\ normal\ cyclic\ prefix \\ 2 \cdot \lceil N_g \, (N_{RB}^{DL} / 8) \rceil & for\ extended\ cyclic\ prefix \end{cases}$$

N_g is a parameter provided by the upper layer, which can be 1/6, 1/2, 1 or 2. Factor m_i depends on the subframe number and the Uplink-Downlink configuration type, which is shown in Table 5.3.

PHICH and PDCCH share control region. The bigger N_g can support a larger quantity of HARQ feedbacks, however, that benefit comes at the expense of PDCCH channel capacity. The situation is especially severe when control region size is small, i.e. CFI value is configured to be small and transmission bandwidth is limited.

Table 5.3: Factor m_i for LTE-TDD configurations [21]

Uplink-Downlink configuration	Subframe number									
	0	1	2	3	4	5	6	7	8	9
0	2	1	-	-	-	2	1	-	-	-
1	0	1	-	-	1	0	1	-	-	1
2	0	0	-	1	0	0	0	-	1	0
3	1	0	-	-	-	0	0	0	1	1
4	0	0	-	-	0	0	0	0	1	1
5	0	0	-	0	0	0	0	0	1	0
6	1	1	-	-	-	1	1	-	-	1

Under normal cyclic prefix, a PHICH group can support up to 8 PHICHs multiplexing used, while under extended cyclic prefix, it can only support up to 4 PHICHs. Table 5.4 lists the orthogonal sequences used.

Table 5.4: Orthogonal sequence for PHICHs in the same group [21]

Sequence index n_{PHICH}^{seq}	Orthogonal sequence	
	Normal cyclic prefix	Extended cyclic prefix
0	$[+1 \quad +1 \quad +1 \quad +1]$	$[+1 \quad +1]$
1	$[+1 \quad -1 \quad +1 \quad -1]$	$[+1 \quad -1]$
2	$[+1 \quad +1 \quad -1 \quad -1]$	$[+j \quad +j]$
3	$[+1 \quad -1 \quad -1 \quad +1]$	$[+j \quad -j]$
4	$[+j \quad +j \quad +j \quad +j]$	-
5	$[+j \quad -j \quad +j \quad -j]$	-
6	$[+j \quad +j \quad -j \quad -j]$	-
7	$[+j \quad -j \quad -j \quad +j]$	-

The actual HARQ information a PHICH carries is only one bit, either 1 (positive acknowledgement) or 0 (negative acknowledgement). The one-bit ACK/NACK will be repeated three times. The repeated sequence is modulated into 3 complex-valued BPSK symbols. All of them are multiplied by one orthogonal sequence defined in Table 5.4 for frequency spread and then scrambled with a cell-specific scrambling sequence, according to the equations introduced in Chapter 6.9.1 of [21].

For normal cyclic prefix (CP) scenario, spreading factor is 4. A 4-symbol orthogonal sequence is multiplied to the 3-symbol BPSK signal. Thus, a 12-symbol length data will be generated after these procedures.

For extended CP scenario, spreading factor is 2. A 2-symbol orthogonal sequence is used to multiply the 3-symbol BPSK signal. According to equations in Chapter 6.9.2 of [21], adding 0 into the 6-symbol length product will expend it to 12-symbol length, which is same as normal cyclic prefix situation.

Multiple PHICHs within one PHICH group will use the same 12 REs, their corresponding symbols will be added together and mapped onto 3 free REGs that have not been used by PCFICH. The REGs positions in each PHICH group depend on PHICH-Duration and PHICH-Resource parameters configurations. The algorithm for calculating positions is defined in Chapter 6.9.3 of [21].

Extended CP has less PHICHs multiplexed into same REGs, in order to give each one more protection. To settle same number of PHICHs, extended CP needs to occupy more resource compared to normal CP.

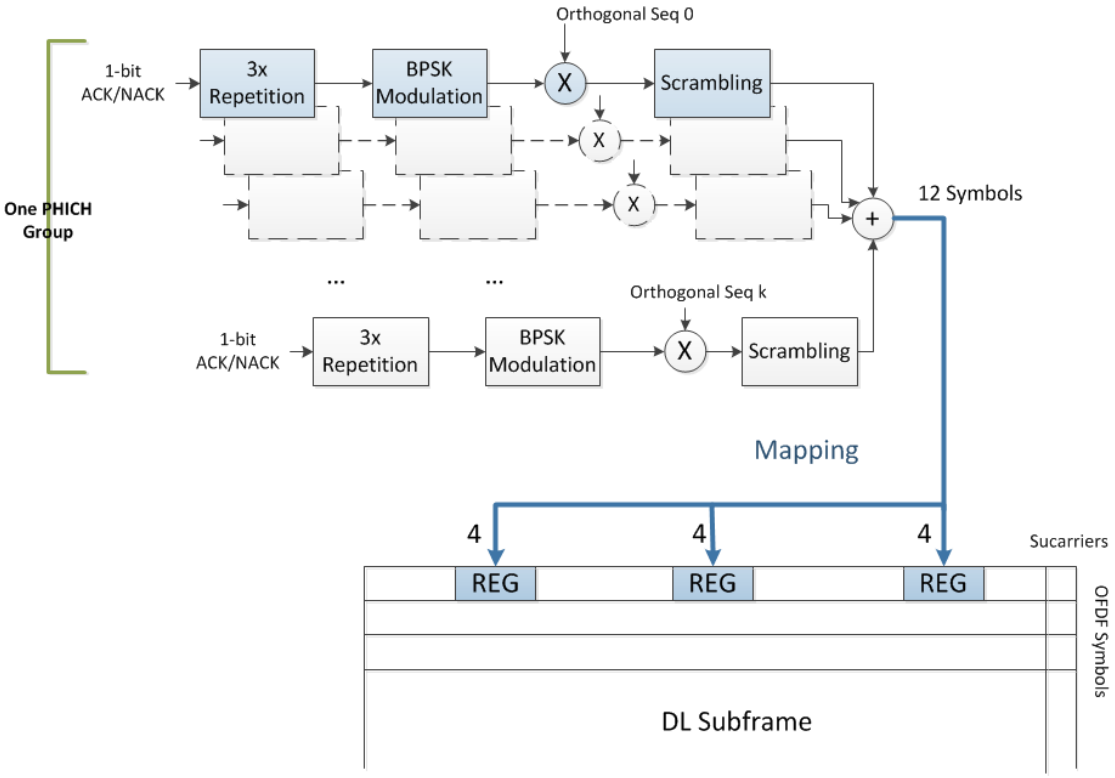

Figure 5.2: PHICH processing procedures (Normal Cyclic Prefix example)

In our tests the PHICH group number is set to 1 and we use normal cyclic prefix. Hence, all together only 3 REGs for all PHICHs (one group) will exist in first OFDM symbol in the DL subframe. The REGs' frequency domain position $\overline{n_i}$ then can be derived as below:

$$\overline{n_i} = \left(N_{ID}^{cell} + \lfloor i * n_{1'}/3 \rfloor\right) mod\ n_{1'} \qquad i = 0, 1, 2$$

$n_{1'}$ is the free REGs number in first OFDM symbol that have not been occupied by PCFICH. Three REGs are uniformly distributed on the first OFDM symbol, with interval of about 1/3 DL bandwidth. Figure 5.2 describes the PHICHs coding, multiplexing and mapping procedures.

5.3 PDCCH

Physical Downlink Control Channel (PDCCH) is allocated into first 1 to 3 OFDM symbols of the corresponding subframe. The number of symbols used is defined by CFI values carried in PCFICH channel. Their relation has been introduced in Chapter 5.1.

PDCCH is used by eNodeB for carrying Downlink control signaling, also known as DCI message. The DCI messages will contain the Downlink resource scheduling information for the current subframe, Uplink resource assignment for the UE, Uplink Transmit Power Control (TPC) command, etc. The DCI bits are protected by 16-bit Cyclic Redundancy Check (CRC) code and tail biting convolutional code. After convolutional encoding, the bits are rate matched and modulated into QPSK symbols. The complex-valued symbols are mapped into the physical resource grid of the subframe. The whole procedure from DCI bits to PDCCH symbol mapping is displayed in Figure 5.3 below:

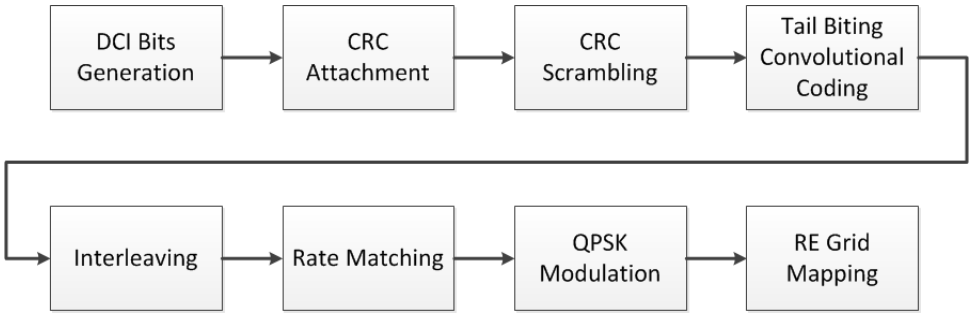

Figure 5.3: PDCCH physical layer procedures

LTE supports four different PDCCH formats, defined in Chapter 6.8.1 of [21]. The formats are listed in Table 5.5 below. Each format will double the size of previous format, containing more cyclic redundancy. The largest format gives the best protection against interference.

Table 5.5: Supported PDCCH formats

PDCCH format	CCEs number	REGs number	REs number	Bits can load
0	1	9	36	72
1	2	18	72	144
2	4	36	144	288
3	8	72	288	576

5.3.1 DCI

As introduced above, DCI is the PDCCH payload content. 3GPP LTE specification Release -8 defines various DCI formats [29] for control signaling in different usage area, summarized in Table 5.6:

Table 5.6: 3GPP LTE release-8 supported DCI format and corresponding usage area

DCI format	DCI format usage area
0	Physical Uplink Shared Channel (PUSCH) scheduling
1	PDSCH scheduling in Single Input Multiple Output (SIMO) scenario
1A	PDSCH compact scheduling in SIMO scenario and random access procedure
2B	PDSCH compact scheduling in Multiple Input Multiple Output (MIMO) scenario
1C	PDSCH very compact scheduling
1D	PDSCH compact scheduling with power offset and precoding
2	PDSCH scheduling with closed-loop MIMO
2A	PDSCH scheduling with open-loop MIMO
3	sending TPC commands for Physical Uplink Control Channel (PUCCH) and PUSCH

The number of DIC bits is format specific. However even identical formats could have different numbers of bits regarding different transmission bandwidths. Within one subframe,

eNodeB may send several DCIs for different UEs at the same time. Also, one subframe can contain multiple different types of DCI that are all sent to one UE.

In this thesis, we use DCI format 0 only. The bits of it, $[a_0, a_1, \dots, a_{A-1}]$, consist of control signaling features which are coded according to Chapter 5.3.3.1.1 in [29]:

1 bit: Differentiation of format 0 and format 1A. Value of 0 will inform UE the received DCI is format 0, or oppositely it is format 1A in case value of 1 is detected.

1 bit: Used as hopping flag.

$\lceil log_2 (N_{RB}^{UL}(N_{RB}^{UL} + 1)/ 2) \rceil$ bits: Used for resource block assignment and hopping resource allocation.

5 bits: Indicating the modulation used and type of redundancy.

1 bit: Indicating whether it is new data.

2 bits: Transmission power control for PUSCH.

3 bits: Cyclic shift for Demodulation Reference Signal (DMRS) used in PUSCH.

2 bits: UL index if using TDD Downlink-Uplink configuration 0. Or Downlink assignment index for other TDD Downlink-Uplink configurations.

1 bit: Channel Quality Indication (CQI) request.

During the test we use 3MHz (15 RB) DL and UL bandwidth, all together 23 bits will be contained in a Format 0 DCI.

5.3.2 DCI Channel Coding and Rate Matching

The DCI bits $[a_0, a_1, \dots, a_{A-1}]$ will be protected by a 16-bit CRC attachment $[p_0, p_1, \dots, p_{15}]$ at the end of sequence, prior to the channel coding. This procedure is designed to provide error detection functionality on UE during DCI decoding process.

The CRC is generated by the length-16 generator polynomial, defined by:

$$g_{CRC16}(D) = [D^{16} + D^{12} + D^5 + 1]$$

The generation is done by first extending the DCI bits with 16 zeros and then dividing the data bits by the polynomial $g_{CRC16}(D)$, follows the rule of module-2 division. After division the zero bits will be replace by 16 bits reminder $[p_0, p_1, \dots, p_{15}]$. The combination of

original data bits and the 16-bit reminder, $[b_0, b_1, \dots, b_{A+15}]$, will be channel coded afterwards.

At the receiver side the UE divides the received data bits $[b'_0, b'_1, \dots, b'_{A+15}]$ by the same polynomial $g_{CRC16}(D)$. The correct received bits sequence will yield to a remainder identical to 0. Otherwise, even 1 bit error in reception will yield to an un-zero remainder, indicating the failure of CRC check.

By using CRC check, UE can distinguish whether DCI bits have correctly decoded and whether the retransmission of corresponding PDCCH is required. In order to enable UE to identify its own PDCCH from others, CRC bits will be scrambled with a 16-bit UE RNTI sequence $\langle x_{rnti,0}, x_{rnti,1}, \dots, x_{rnti,15} \rangle$, according to equations below [29]. It leads to a new sequence $[c_0, c_1, \dots, c_{A+15}]$. RNTI stands for Radio Network Temporary Identifier number.

$$c_k = \begin{cases} b_k & (k = 0, 1, 2, \dots, A-1) \\ (b_k + x_{rnti,k-A}) mod\ 2 & (k = A, A+1, A+2, \dots, A+15) \end{cases}$$

In case MIMO is also configured on UE, an additional scrambling function will be deployed. UE antenna selection mask $\langle x_{AS,0}, x_{AS,1}, \dots, x_{AS,15} \rangle$ is used to distinguish different antenna ports.

$$c_k = \begin{cases} b_k & (k = 0, 1, 2, \dots, A-1) \\ (b_k + x_{rnti,k-A} + x_{AS,k-A}) mod\ 2 & (k = A, A+1, A+2, \dots, A+15) \end{cases}$$

$$\langle x_{AS,0}, x_{AS,1}, \dots, x_{AS,15} \rangle = \begin{cases} \langle 0,0,0,0,0,0,0,0,0,0,0,0,0,0,0,0 \rangle & UE\ antenna\ port0 \\ \langle 0,0,0,0,0,0,0,0,0,0,0,0,0,0,0,1 \rangle & UE\ antenna\ port1 \end{cases}$$

During reception procedure, UE can identify whether the PDCCH in decoding attempt is for itself by conducting CRC checking on the descrambled bits sequence.

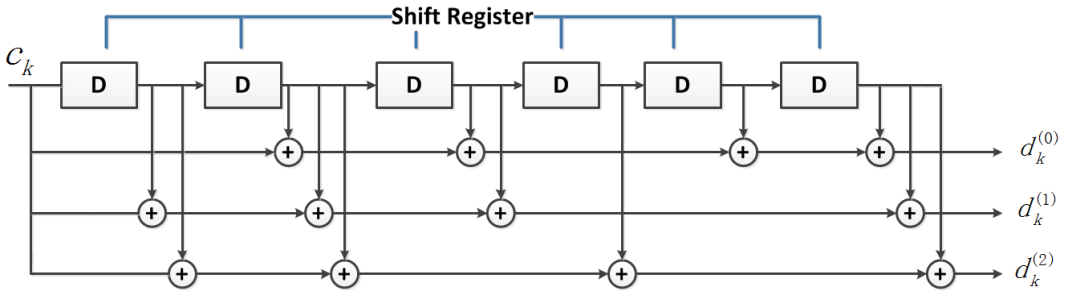

Figure 5.4: 1/3 Code Rate Tail Biting Convolutional Encoder

The CRC extended DCI bits are channel coded with tail biting convolutional code. The LTE specification uses 1/3 code rate with constraint length 7. The encoder configuration is illustrated in Figure 5.4.

At the beginning, the 6-bit shift register will be initialized with the last 6 bits of input sequence, here means $[c_{A+10}, c_{A+11}, \dots, c_{A+15}]$. The encoder will generate three output streams, $d_k^{(0)}$, $d_k^{(1)}$ and $d_k^{(2)}$. Within each step k, output $d_k^{(i)}$ is calculated by summing up input bit c_k with the bits in the register as Figure 5.4 shown. Afterwards, register will shift right one bit, and insert the c_k into the first left bit of register. The three output streams have the same size $A + 16$. They will be collected one after the other and interleaved according to algorithm introduced in Chapter 5.1.4 of [29], leading to bits sequence $[w_0, w_1, \dots, w_{3A+47}]$.

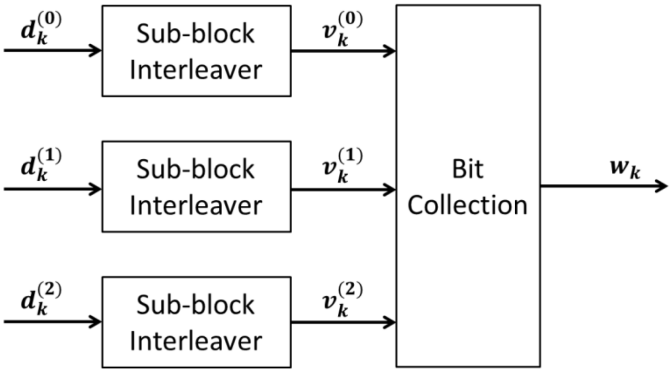

Figure 5.5: Interleaving and bit collection blocks of PDCCH

After channel coding, QPSK modulation will be used for transforming bits sequence into complex-valued symbols that are mapped into RE grid. Since the encoded bits are QPSK coded, one symbol on an RE contains two encoded bits information.

The LTE specification introduces a concept called “Aggregation Level” that describes how big space a PDCCH is mapped into. Four different aggregation levels: 1, 2, 4 and 8 are defined. They represent corresponding CCE numbers used for mapping, being able to load 72, 144, 288 and 576 bits information respectively.

The eNodeB needs to choose an aggregation level with sufficient size to map all bits after bit collection procedure. However, the minimum size is not always the best choice. Considering of the channel quality, eNodeB may choose to use a higher aggregation level to provide better bits protection. Higher aggregation levels use cyclic repetition of encoded bits $[w_0, w_1, \dots, w_{3A+47}]$ and map the resulting bits into a larger number of REs. The repeated bits will occupy all the REs corresponding to chosen aggregation level. This procedure is called rate matching, leading to the new bits sequence $[e_0, e_1, \dots, e_E]$ afterwards. The redundancy added during such process will enhance the PDCCH robustness against bad channel quality and maintain the successful decoding rate on UE at a desired level.

5.3.3 PDCCH Symbols Mapping

The bit sequence $[e_0, e_1, \dots, e_E]$ will be QPSK modulated. The encoded complex-valued PDCCH symbols are mapped onto CCEs arranged for them. Unlike PCFICH and PHICH mapping that can calculate scheduled REGs' positions directly, PDCCH symbols mapping is based on the availability of REGs in a given subframe. Before conducting the actual mapping, the eNodeB is required to count the total number of free REGs left in control region. These are REGs that have not been occupied by PCFICH or PHICH. Such free REGs will be numbered from 0 to $N_{REG} - 1$.

The REGs are indexed by a specific algorithm in Chapter 6.5.8 of [21]. The pseudo code below describes the indexing procedure, where the address of nth REG is represented by (k, l). k represents the subcarrier index and l represents OFDM symbol index.

start with $n = 0$

for $k = 0$ to $N_{RB}^{DL} * N_{sc}^{RB} - 1$, increases k by 1 after each iteration

for $l = 0$ to $Control\ Region\ Symbol\ Number - 1$, increases l by 1 after each iteration

if RE (k, l) is free, an REG starts from it is indexed as nth REG. This REG consists of 4 consecutive free REs starts from (k, l) by increasing l

$n = n + 1$

end

end

end

The total number of available CCEs inside a subframe can be calculated based on

$$N_{CCE} = \lfloor N_{REG} / 9 \rfloor .$$

These CCE are numbered from 0 to $N_{CCE} - 1$. The remaining REGs will not be used. The available CCEs define the amount of resources available for allocating PDCCH messages. It may happen that not all the CCEs are used by PDCCH. The unused CCEs are filled with "NIL" and no power is transmitted on REs of those CCEs.

An example of PDCCH allocation is illustrated in Figure 5.6, showing the indexing of REGs in the first two RBs of the control region. The control region spans 4 OFDM symbols. In the first symbol there are two free REGs, in the rest of symbols we can each allocate six free REGs. However, REGs in first OFDM symbol are not indexed as No.1 and No.2. The first REG is located into second OFDM symbol while the second one is located into third OFDM symbol. Nine consecutive REGs will then form a CCE for PDCCH allocating.

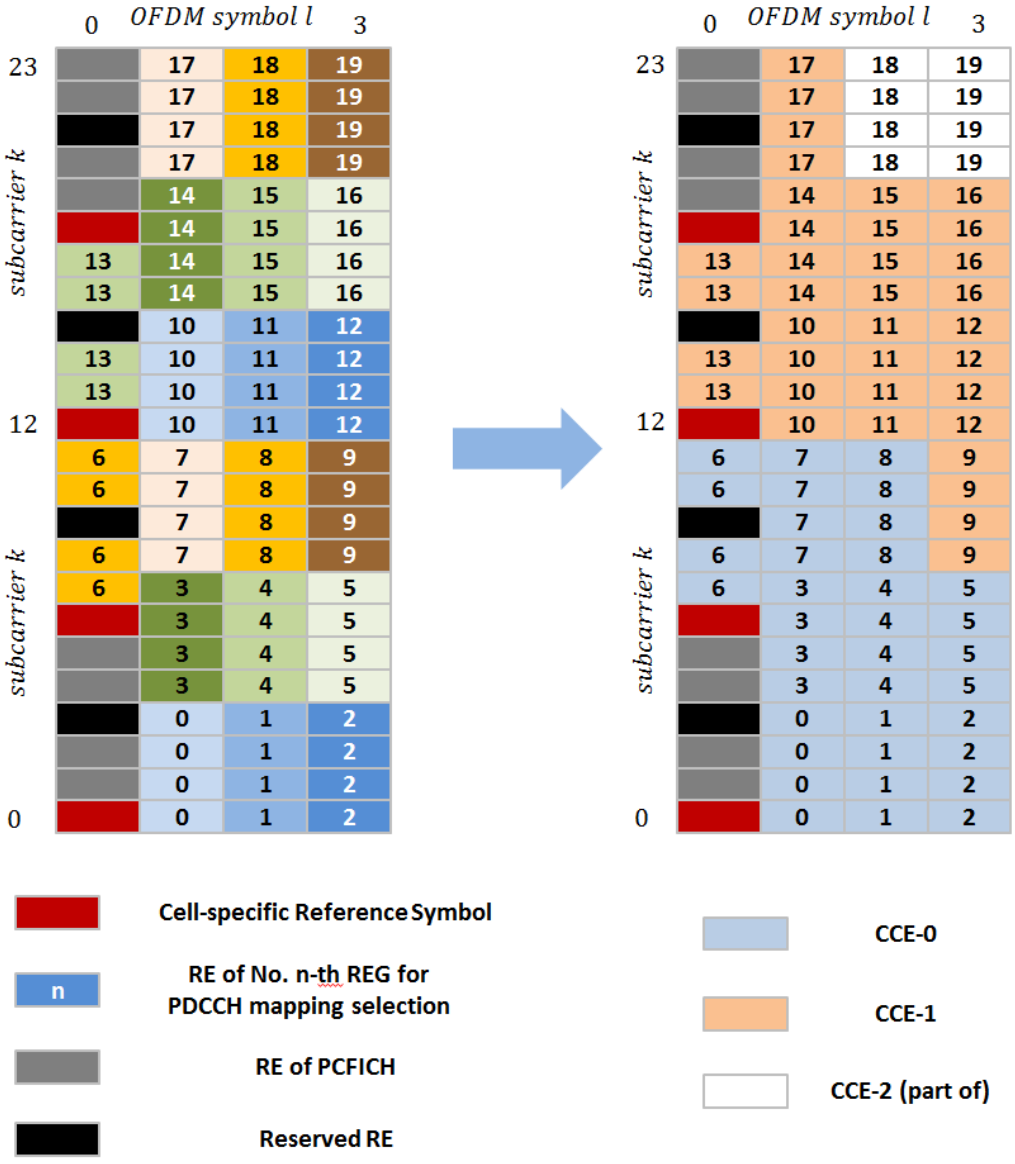

Figure 5.6: REG indexing and CCE calculation for PDCCH

In large transmission bandwidth condition, eNodeB can allocate many PDCCH messages. The UE does not know the format and configuration of the DCI messages, i.e. the UE is unaware of PDCCH size and position inside the control region. To avoid missing even one PDCCH, the UE blindly searches through all possible positions in control region that potential

PDCCHs may exist. In order to simplify eNodeB scheduling procedure, and even more important, in order to decrease UE blind searching trials, LTE specification introduces rules for allocating PDCCH on selectable mapping positions (Chapter 9.1 of [30]). The corresponding UE blind decoding procedure of PDCCH will be explained later in Chapter 6.

The available CCEs area can be divided into common search space and UE-specific search space. The common search space contains as much as 16 CCEs, which will start from first available CCE. The common search space is used for sending control information which is common for all UEs. The UE-specific search space is used for sending information for particular UE. These two spaces may overlap. However, if system CCE number is smaller than 16, all the CCEs will be configured as common search space. The size of both spaces is limited depends on aggregation level, shown in Table 5.7. A possible PDCCH mapping position is called PDCCH candidate, which is also a position UE will try blindly decoding.

Table 5.7: Common and UE-Specific searching space size [30]

Type	Aggregation Level	Size (in CCEs)	Number of PDCCH candidates
Common search space	4	16	4
	8	16	2
UE-specific search space	1	6	6
	2	12	6
	4	8	2
	8	16	2

When aggregation level 1 or 2 is set, only a UE-specific search space exists. On contrary, common search space and UE-specific search space will co-exist while using aggregation level 4 or 8. PDCCH symbols are mapping according to following algorithm:

First, for a PDCCH with size of n CCE, it can only start mapping from a CCE with index a that fulfills $a\ mod\ n = 0$. The options number hence will be limited.

Second, the CCE indexes for a PDCCH should equal to the values from the formula:

$$L * \{(Y_k + m) mod \lfloor N_{CCE,k}/L \rfloor\} + i$$

Within which $L \in \{1, 2, 4, 8\}$ is the aggregation level set. $i = 0, 1, \dots L-1$. $m = 0, 1, \dots, M^{(L)} - 1$, $M^{(L)}$ is PDCCH candidates number defined in Table 5.7 above. k is the subframe number, ranges from 0 to 9. $N_{CCE,k}$ is the total CCEs number in subframe k. Y_k is iteratively calculated from:

$$Y_k = (A * Y_{k-1})\ mod\ D$$

Within which, initial value $Y_{-1} = n_{RNTI} \neq 0$, $A = 39827$, $D = 65537$. n_{RNTI} is Radio Network Temporary Identity number. Y_k is constantly set to 0 in common search space.

For example, if aggregation level $L = 4$, subframe number $k = 1$, $N_{CCE,1} = 23$, at UE-specific searching space, $n_{RNTI} = 5$. Then

$$Y_0 = (39827 * 5)\ mod\ 65537 = 2524,$$

$$Y_1 = (39827 * 2524)\ mod\ 65537 = 55127.$$

$$L * \{(Y_1 + m) mod \lfloor N_{CCE,1}/L \rfloor\} + i$$

$$= 4 * \{(55127 + m) mod\ 5\} + i, \quad i = \{0, 1, 2, 3\}, \quad m = \{0, 1\}$$

Hence, we can know that 2 possible PDCCH candidates exist, they are CCEs with indexes of $\{8, 9, 10, 11\}$ and $\{12, 13, 14, 15\}$ respectively.

If the eNodeB wants to map a PDCCH in UE-specific search space, but all possible PDCCH candidates are unavailable, e.g. partially or fully occupied by other prior allocated PDCCHs, eNodeB can instead map this PDCCH into common search space.

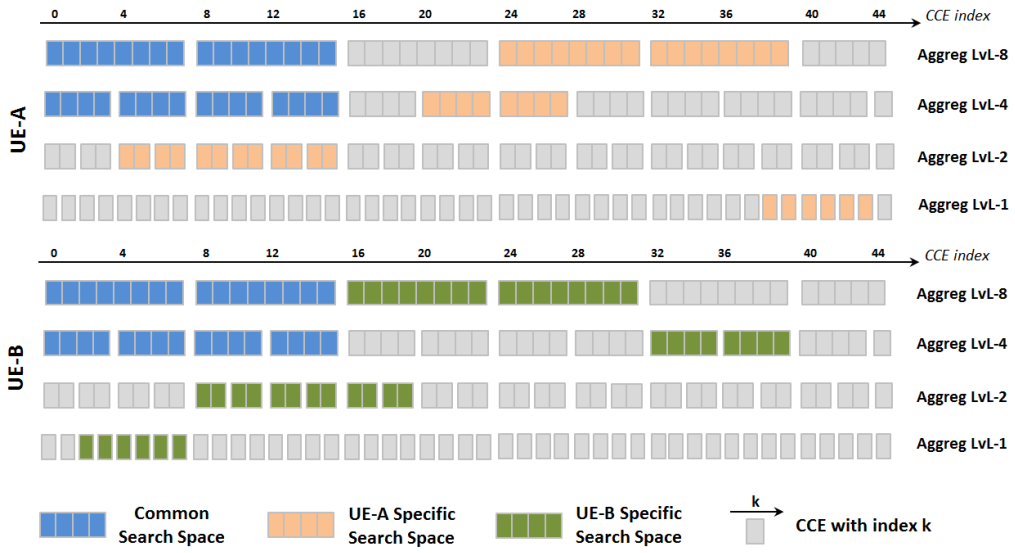

Figure 5.7: A PDCCH searching space example

A PDCCH search space example is shown in Figure 5.7, in which the eNodeB maps PDCCHs for UE-A and UE-B. Total CCE number is 45. In UE-A's specific search space, if eNodeB maps a PDCCH of aggregation level 8 for UE-A firstly at a candidate position that consists of CCEs with indexes $\{24 \sim 31\}$, then it cannot map another aggregation level 4 PDCCH for UE-A at CCEs with indexes $\{24 \sim 27\}$ due to overlapping. The eNodeB can either

choose CCEs with indexes $\{20 \sim 23\}$, or in case overlapping still exist, choose CCEs of indexes $\{0 \sim 3\}$, indexes $\{4 \sim 7\}$, indexes $\{8 \sim 11\}$ or indexes $\{12 \sim 15\}$ in common searching space instead. Similarly if eNodeB maps an UE specific PDCCH of aggregation level 8 at CCEs with indexes $\{24 \sim 31\}$ for UE-B firstly, then it cannot map a PDCCH for UE-A at any candidates that contain a CCE with index of $\{24 \sim 31\}$. Thereby, it should choose an un-overlapped candidate in UE specific searching space, or alternatively one in common searching space.

5.4 PDSCH

Physical Downlink Shared Channel (PDSCH) is utilized for transmitting Downlink Share Channel (DL-SCH) in transport layer that carries the Downlink data for UE. PDSCH region starts from the OFDM symbol next to the last ODFM symbol of the control region. In subframe 1 and subframe 6, due to the presence of Primary Synchronization Signal (PSS), the OFDM symbol 2 cannot be used by PDSCH. Similarly, due to the presence of Secondary Synchronization Signal (SSS) in the subframes 0 and subframe 5, PDSCH cannot use a part of last symbol in these subframes.

The PDSCH payload, DL-SCH bits $[a_0, a_1, \dots, a_{A-1}]$ will respectively undergo CRC attachment, code block segmentation, code block CRC attachment, channel coding, rate matching and block concatenation during physical layer processing. Unlike control channels, PDSCH can choose QPSK, QAM16 or QAM64 as modulation scheme, for providing diverse data rates selection.

The modulated complex-valued symbols will be mapped into data region of the DL subframe.

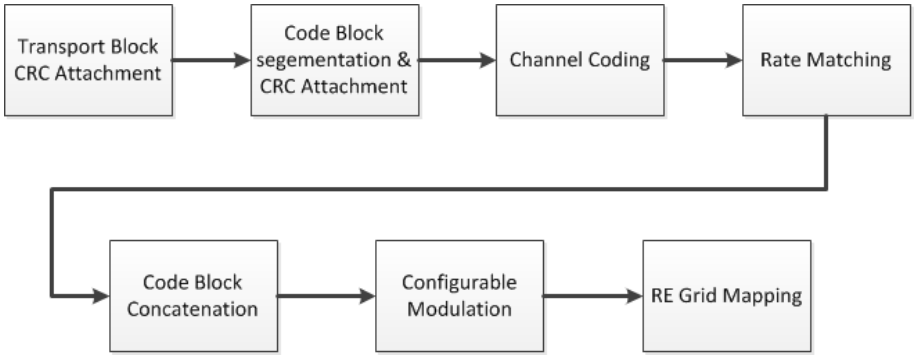

Figure 5.8: PDSCH physical layer procedures

Chapter 6

UE Downlink Decoding Procedures

For UE, the Downlink decoding is processed as an inverse procedure compared to eNodeB encoding. The UE uses decoded PDCCH for getting instruction of decoding data in PDSCH or for receiving scheduling grants of PUSCH.

The UE processing starts by decoding PCFICH. It is a reverse procedure of eNodeB encoding it. After that UE will know how many OFDM symbols are configured for control region. The PCFICH is always located in the first OFDM symbol. Its REG's position depends on the Cell Identity number. After decoding PCFICH, UE proceeds with checking PHICH and identifying the ACK/NACK of Uplink data.

The most sophisticated process for control channels is the decoding of PDCCH. Since UE does not know which message was sent, it uses blind decoding strategy. Considering multiple PDCCH candidates exist, UE is unaware of PDCCH position, aggregation level and DCI format. In addition, as analyzed in Chapter 5.3, more than one PDCCH for a single UE may coexist within a subframe. Thereby, UE needs to search through all potential positions with all possible sizes to ensure capturing all the transmitted PDCCH messages. The structure of common search space and UE-specific search space helps to narrow down the blind decoding trials.

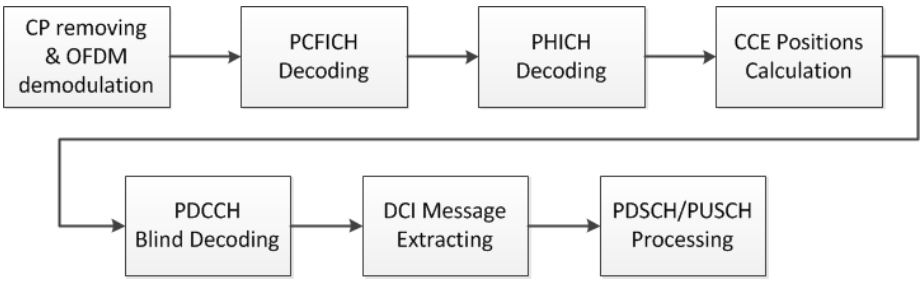

Figure 6.1: UE Downlink physical layer decoding procedures

Figure 6.1 illustrates the DL physical layer decoding procedures. Below we introduce the basic content of each step.

Step 1. Decode OFDM symbols in received subframe and recover complex-valued symbols in them. In a DL subframe, the receiver removes the cyclic prefix and performs N-Point FFT. If the delay of a multi-path component is within the size of cyclic prefix, it can be successfully decoded.

Step 2. Decode the PCFICH and obtain the CFI value. This step is conducted using correlation detection. The correlator checks for three different 32-bit codewords $B_n = < b_{n,0}, b_{n,1}, \dots, b_{n,31} >, (n = 1,2,3)$, which introduced in Table 5.2. The positions of the codeword's REGs are computed using the same algorithm that eNodeB used for PCFICH allocation. After QPSK demodulation and descrambling (Cell ID), estimate of the codeword $B' = < b'_0, b'_1, \dots, b'_{31} >$ is obtained. Respectively multiplying B' by B_n, $(n = 1,2,3)$, UE can determine the CFI value. The determined CFI value should ensure the maximum correlation result.

$$max(B' * B_n) = max \sum_{k=0}^{31} \left(b'_k * b_{n,k}\right), \quad n = 1,2,3$$

Step 3. Decode the PHICH, obtain the ACK/NACK of physical layer H-ARQ. UE uses the same algorithm as described in Chapter 5.2, finding PHICH group's REGs position from received subframe, based on its own n_{PHICH}^{group} value.

For a system with one PHICH group and normal cyclic prefix, if eNodeB send three repeated modulated ACK/NACK symbols $< a_m, a_m, a_m >$, 12 complex-valued PHICH symbols (distributed in 3 REGs) will be retrieved by UE from first OFDM symbol in DL subframe, marked as $< \hat{a}_1, \hat{a}_2, \dots, \hat{a}_{12} >$. As shown in Table 5.4, $S_k = < s_{k,1}, s_{k,2}, s_{k,3}, s_{k,4} >$, $(k = 0,1, \dots, 7)$ are orthogonal sequences used in one PHICH group.

$$< \hat{a}_1, \hat{a}_2, \dots, \hat{a}_{12} > = \sum_{k=0}^{7} (< a_k, a_k, a_k > \times S_k)$$

$S_m = < s_{m,1}, s_{m,2}, s_{m,3}, s_{m,4} >$ sequence corresponding to UE's own n_{PHICH}^{seq} will help split 3-Symbol codeword from other multiplexed ones, due to sequence orthogonality.

$$< \hat{a}_1, \hat{a}_2, \dots, \hat{a}_{12} > * < S_m, S_m, S_m >$$

$$= \left\{ \sum_{k=0}^{7} (< a_k, a_k, a_k > \times S_k) \right\} * < S_m, S_m, S_m >$$

$$= < a_m\ S_m * S_m,\ \ a_m\ S_m * S_m,\ \ a_m\ S_m * S_m >$$

$$+ \sum_{k \neq m} < a_k\ S_k * S_m,\ \ a_k\ S_k * S_m,\ \ a_k\ S_k * S_m >$$

$$= \delta < a_k, a_k, a_k > + 0$$

$$\delta = S_m * S_m = \sum_{i=1}^{4} \left(s_{m,i} * s_{m,i}\right)$$

Depends on the sequence used, δ can be ± 4. Demodulate the codeword $< a_k, a_k, a_k >$ with BPSK scheme, UE will get the three repeated ACK/NACK bits.

Step 4. Conduct CCE indexing. According to the CFI value obtained in Step 2, UE knows the size of the control region. It will count all REs within it that have not been occupied by reference symbols, PCFICH or PHICH, etc. Using the same algorithm that eNodeB used during REG and CCE indexing, UE obtains the CCEs number and positions.

Step 5. Blind PDCCH decoding. As explained in Chapter 5.3.3, PDCCHs are mapped into UE-specific space and common space. UE will try decoding in both spaces on all candidate code positions, regarding all possible DCI formats and aggregation levels.

For the searching of format k DCI, of which length is $M_{DCI(k)}$, UE will first check through the common searching space, starts with candidates of aggregation level 8, then on those of aggregation level 4. After that UE-Specific Searching Space will be checked, start from candidates of aggregation level 8 to those of level 1. The 16-bit CRC attachment is used for determining whether PDCCH exists on each candidate position.

At each blind attempt, complex-valued symbols set of candidate i is:

$$< \hat{a}_i(0), \hat{a}_i(1), \dots, \hat{a}_i(N_{g,i} - 1) >$$

$N_{g,i}$ indicates the symbols number at aggregation level g. The corresponding bits set after QPSK demodulation is expressed below, $2N_{g,i}$ is the bits number.

$$< b_i(0), b_i(1), \dots, b_i(2N_{g,i} - 1) >$$

Since bits length of DCI format k is $M_{DCI(k)}$, after tail biting convolutional encoding, its length is $N_c = 3(M_{DCI(k)} + 16)$, where we consider 16-bit CRC attachment. These bits will be repeated several times for fulfilling current aggregation level required length. The repeat time can be calculated by:

$$T = \left\lfloor 2N_{g,i} / (3M_{DCI(k)} + 48) \right\rfloor$$

The higher aggregation level it is, the lager space can be provided for big size DCI format. The more important, under the bad channel conditions, large redundancy of periodical repetition in high aggregation level enhances PDCCH successful decoding rate. If T is zero, it means REs number of current aggregation level is insufficient for target DCI format. UE will directly jump over this aggregation level. Otherwise, UE can find the potential DCI bits. The DCI bits with CRC attached after channel coding is:

$$< c_i(0), c_i(1), \dots, c_i(N_c - 1) >$$

Taking advantage of the bits repetition,

$$\hat{c}_i(n) = \begin{cases} \sum_{l=0}^{T} b_i(n + l * N_c) & 0 \le n \le (2N_{g,i}\ mod\ N_c) - 1 \\ \sum_{l=0}^{T-1} b_i(n + l * N_c) & (2N_{g,i}\ mod\ N_c) \le n \le\ N_c - 1 \end{cases}$$

After de-interleaving and tail biting convolutional decoding, UE will retrieve the DCI and CRC bits:

$$< d_i(0), d_i(1), \dots, d_i\big(M_{DCI(k)} - 1\big), d_{CRC,0}, d_{CRC,1}, \dots, d_{CRC,15} >$$

Descrambling the UE RNTI and removing antenna selection mask from last 16-bit CRC codeword, the outgoing CRC bits $< d'_{CRC,0},\ d'_{CRC,1}, \dots, d'_{CRC,15} >$ will go through CRC check. The CRC check uses the same generator polynomial $g_{CRC16}(D)$ introduced in Chapter 5.3.2. A zero remainder after dividing $< d'_{CRC,0},\ d'_{CRC,1}, \dots, d'_{CRC,15} >$ with the polynomial $g_{CRC16}(D)$ indicates a correct received PDCCH for the UE and UE can proceed with decoding the DCI bits. The data bits $< d_i(0), d_i(1), \dots, d_i\big(M_{DCI(k)} - 1\big) >$ in DCI format k codeword will be passed to upper layer for further processing. The upper layer parses the bits and extracts the information confined in the message. Otherwise, an un-zero remainder reveals the absence of PDCCH on this candidate or an error reception happened.

After finishing one trial, UE will continue iterate to the next PDCCH candidate position until all candidates have been checked through.

Step 6. Extract the embedded message from the successful fetched DCI bits.

Step 7. Decoded DCI message from step 6 carries either PDSCH data allocation and modulation scheme or PUSCH resource grant. Based on the DCI information, UE will be capable of extracting PDSCH data from DL subframe, as well as conducting PUSCH symbols transmission in the authorized resource blocks in the UL subframes.

Chapter 7

LTE-TDD Heterogeneous Network Implementation

In the LTE Downlink physical layer, DL user data is carried by Physical Downlink Shared Channel (PDSCH). PDSCH associates with control signaling carried in PDCCH. The errors in PDCCH also prohibit decoding of data in PDSCH. This thesis focuses on PDCCH performance of macro-cell UE under the co-channel heterogeneous network. We evaluate the performance as a function of co-channel interference strength level. A realistic co-channel heterogeneous network test scenario will be set up and implemented based on USRP devices. In this test network, PDCCH performance measurements will be conducted.

7.1 Co-Channel Heterogeneous Environment Setup

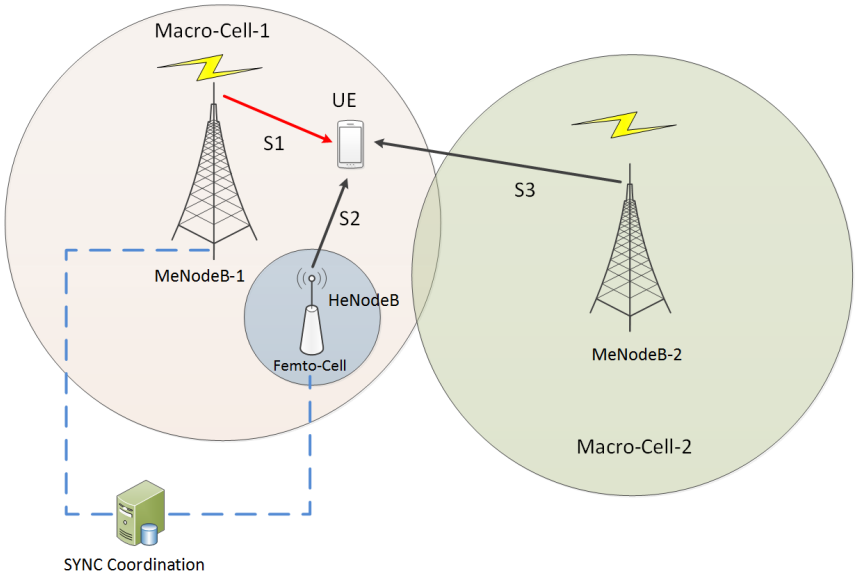

Figure 7.1: Overlaid co-channel transmission test scenario

To simulate a simple co-channel heterogeneous network, we set up a test scenario as displayed in Figure 7.1. The realistic test system contains four nodes. One macro-cell eNodeB works as the primary BS to which the UE is attached. This eNodeB is called MeNodeB-1. The other macrocell MeNodeB-2 works as an adjacent macro-cell. A third node is configured to be a HeNodeB. It provides femto-cell coverage service inside the MeNodeB-1 coverage area.

The UE is communicating with MeNodeB-1. However, its position is close to HeNodeB, of which the signal is received by UE as co-channel interference. The signal from MeNodeB-2 is also received by UE as interference.

Usually in an LTE-TDD heterogeneous network, femto-cell should coordinate the DL/UL switching time and configuration type with macro-cell, in order to avoid the overlapping between their DL subframes and UL subframes. In co-channel environment, the timing mismatched transmission will cast severe interference on the opposite link direction [23]. For example, a macro-cell UE receiving DL data from a distant macro-cell eNodeB may suffer connection blocking if a femto-cell UE nearby is transmitting its UL data with high power.

Research in [31] also indicates that if a macro-cell UE stays close to a femto HeNodeB which has CSG strategy will the UE suffer cell outage problem. The macro-cell UE receives a strong signal from HeNodeB but is refused to access. Meanwhile, it receives a relatively weaker signal from a macro-cell eNodeB that actually serves it. Compared to femto-cell UEs, macro-cell UEs are more vulnerable to the inter-cell interference brought by co-channel heterogeneous deployment.

On the other hand, PDCCH plays an important role in communication. Since the signaling and resource grant information that PDCCH carriers is the prerequisite for a UE to access the data channel (PDSCH). Fail in decoding PDCCH will automatically lead the UE to abandon the data channel content. Considering the PDCCH uses convolutional encoding while the data channel has stronger turbo encoding, the PDCCH is less robust against interference compared to the data channel.

Hence, it is very interesting and meaningful to evaluate the macro-cell PDCCH performance under the co-channel deployed heterogeneous network. We will measure the macro-cell PDCCH reception quality at the macro-cell UE according to the model shown in Figure 7.1. We want to present how well the macro-cell PDCCH can tolerate the co-channel interference and what extent of performance degradation will macro-cell PDCCH suffer. Received PDCCH block error rate (BLER) and PDCCH payload (DCI bits) bit error rate (BER) will be used as the criteria for PDCCH performance measurement.

In a heterogeneous network, providing precise synchronization of eNodeBs radio frame and DL/UL switching moment is a significant challenge. HeNodeB can adopt different

methods to achieve time alignment or synchronization with MeNodeB, like using GPS, adding signaling via core network or synchronize over the air. HeNodeB is usually installed and connected to operator's core network via subscriber's own internet connection. As a consequence, its backhaul signaling traffic quantity and quality cannot compete with the dedicated connection that links macro-cell eNodeB to the core network. Capturing this situation, we use over the air synchronization method in the thesis, since it does not need the support of backhaul signaling and is relatively easy to implement. During DL subframes, HeNodeB works similar to a UE. By tracking the synchronization reference signal (PSS) in MeNodeB-1's subframe, HeNodeB aligns its own radio frame to that of MeNodeB. The drawback of over the air synchronization is that it will significantly increase the HeNodeB system complexity.

In our test set up, Macro-Cell-1 and Macro-Cell-2 belong to the same operator, and they are assigned with different Cell Identity Numbers (Cell-IDs), 0 and 1 respectively. Since HeNodeB may be unaware of the detailed configuration of primary MeNodeB-1, their Cell IDs may happen to be same. In order to test the extreme situation, the identity of femto-cell is set to be same as that of Macro-Cell-1. The Cell-ID provides seeds for spreading codes, and positions of reference signals, PHICH and PCFICH inside the subframe. The same Cell-ID means that the cells have exactly overlapping channel allocations. The transmitters interfere more severely compared to different Cell-ID case.

7.2 USRP Based Implementation

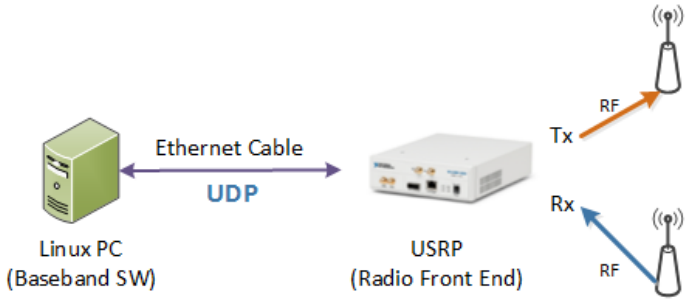

Figure 7.2: USRP based eNodeB and UE implementation

In the experiment, we use the Ettus Research USRP N200 device to work as radio front end, transmitting and receiving RF signals. The ADC/DAC and Up Conversion/Down Conversion of RF signal are also conducted inside USRP. The USRP is connected to a Linux PC (with Ubuntu 12.04) via gigabit Ethernet cable with UDP connection. The digital baseband signal is sent to/received from USRP device. The Linux PC is in charge of running baseband processing code that is implemented by C++ program. The basic approach of using

non-real-time operating system at general purpose processor (GPP) to implement LTE-TDD baseband protocol stack is discussed in [32].

A basic node consists of one USRP and one connected PC, displayed as Figure 7.2, achieving the functionality of a UE or an eNodeB. Our platform baseband processing does not contain layer mapping and precoding procedures. The baseband DL/UL modulated complex-valued symbols will be directly mapped to/recovered from OFDM/SC-FDMA symbols. Our test uses 2.4 GHz center frequency, with 3MHz channel bandwidth, corresponding to 15 RBs transmission bandwidth.

Three USRP based eNodeB and one UE are deployed to compose a realistic co-channel heterogeneous network. Figure 7.3 displays the device connections set up. All USRP Tx signals use the same output power levels. All eNodeBs/UE use LTE-TDD DL/UL configuration-5 (10 subframes inside one radio frame are assigned as D-S-U-U-U-D-D-D-D-D).

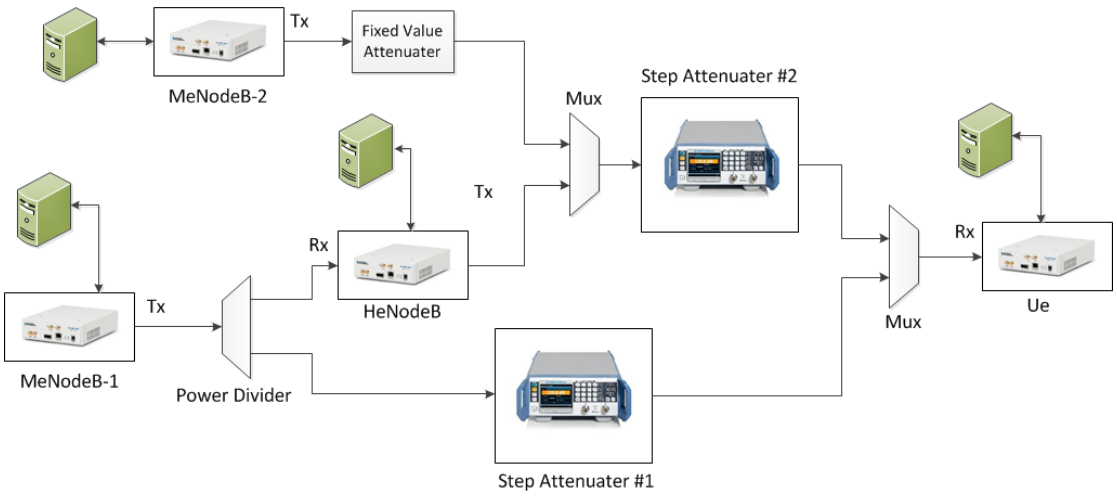

Figure 7.3: Device connections to model co-channel transmission

In order to guarantee precise control on SINR, the USRP devices do not transmit over the air but are connected through the coaxial cables. The DL signal from MeNodeB-1 is split into two sub-routes by a 3dB power divider. One path is connected to UE Rx port, working as the normal DL data link. The other path is linked to HeNodeB Rx port. It is used by HeNodeB as the frame timing alignment reference signal.

A fixed value attenuator (16dB) is connected with the MeNodeB-2 Tx terminal, which simulates signal loss from it to the macro-cell due to distance. Step attenuator #1 is used to weaken DL MeNodeB-1 Tx signal, adjusting SINR level of received signal at UE. HeNodeB is deployed inside the house, and UE in macro-cell locates outside the house. Hence, step attenuator #2 is configured onto DL from HeNodeB to UE, in order to simulate the different levels through-wall penetration loss of the HeNodeB Tx signal received by UE. In our test, the

attenuation is set to be 20dB and 40dB respectively, adjusting the influence brought by femto-cell to macro-cell.

HeNodeB is designed to coordinate its transmission with overlaid MeNodeB-1. The idea of this kind of time synchronization is to enforce HeNodeB keep tracking PSS signal in MeNodeB-1's DL subframe, conducting radio frame time alignment. This working mode helps eliminate the UL/DL overlapping interference between femto-cell and macro-cell. Under this mode, HeNodeB DL and MeNodeB-1 UL subframes will not overlap, neither will HeNodeB UL and MeNodeB-1 DL subframes.

7.3 Control Group with Single eNodeB

In the co-channel heterogeneous deployment of HeNodeB and MeNodeB, the transmission of HeNodeB inside a building will always cause co-channel interference to the macro-cell. In general, the penetration loss due to building walls can only alleviate the interference level but will not totally remove it.

In order to compare the PDCCH performance degradation in heterogeneous co-channel transmission versus ideal transmission, we set up a single eNodeB environment as the control group, for simulating an ideal environment that contains no inter-cell interference. In this case, HeNodeB and MeNodeB-2 are not present.

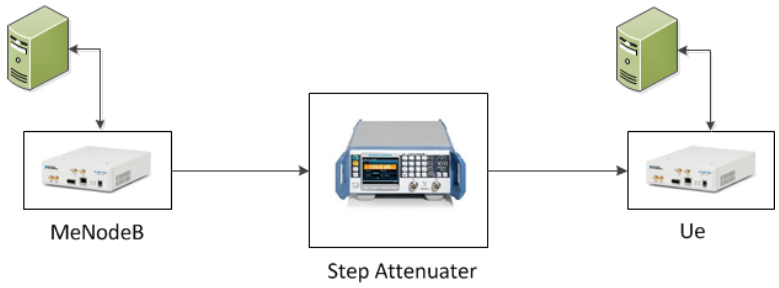

Figure 7.4: Single eNodeB transmission scenario

For simplicity, a system consists of one eNodeB and one UE is used, shown in Figure 7.4. A macro-cell MeNodeB is directly connected to UE via coaxial cable. A step attenuator inside the DL signal path is configured to control the UE received signal SINR level.

We will study the comparison between single eNodeB transmission and co-channel heterogeneous transmission. The results are presented in the next chapter.

Chapter 8

Measurement and Result Analysis

This chapter will present the PDCCH measurement results in single eNodeB transmission scenario and heterogeneous network scenario respectively. A comparison between PDCCH in two scenarios will be performed. Based on the results and shortcoming analysis of current configurations, a proposal of system improvement and the future test will be given at last.

8.1 Measurement Configuration

As discussed in Chapter 7, we focus on the macro-cell PDCCH performance under heterogeneous network deployment. We use block error rate (BLER) of UE received PDCCH and bit error rate (BER) of PDCCH payload bits (DCI) as the evaluation criteria. In heterogeneous network scenario, the PDCCH is sent from macro cell MeNodeB-1 to the UE. In single eNodeB scenario, the PDCCH is sent from MeNodeB to the UE.

In order to maintain consistency, we only use CFI = 3 and DCI format 0 in the test. We measure the PDCCH performance with all four aggregation levels. The DCI and corresponding coded bits length in the test are displayed in Table 8.1.

A special case is using aggregation level 1, which marked with a star in Table 8.1. In aggregation level 1, the available space to load one PDCCH is 1 CCE, which equals to 9 REGs or 36REs. Since PDCCH is QPSK modulated, it can load 72 bits. As channel coding will triple the bits stream size, 72 bits space can only be used by 24 bits information before channel encoding. Consider DCI is also attached with 16-bit CRC at the rear, the available payload for DCI data is only 8 bits. This size can be used for a small length DCI format (e.g. DCI format 1C in 1.4MHz bandwidth can be 8 bits length). However, the DCI format 0 used in test up is 23 bits length.

Regarding evaluating PDCCH performance, we are not interested in the exact content represented by each bit of a DCI, but just want to measure whether the DCI bits as an entity has been correctly received. The correctness is only related with CRC and channel coding but

not the content inside DCI. Hence, for aggregation level 1 evaluation, we only take first 8 out of 23 bits of DCI format 0 in use. These 8 bits will be attached CRC as well as channel coded like situations in other aggregation levels. After then it can be fit into 1 CCE.

Table 8.1: DCI bits size used under different aggregation levels in our test

Aggregation Level	Support REG Number	Available Bits Size for a PDCCH	DCI Bits Size (Plus CRC) before channel coding	DCI Bits Size Used in Test
1	9	72	24	8 *
2	18	144	39	23
4	36	288	39	23
8	72	576	39	23

Other aggregation levels have enough space to support a full-size format 0 DCI. The spaces of aggregation level 2, aggregation level 4 and aggregation level 8 are bigger than a format 0 DCI requires, hence coded DCI symbols will be repetition coded to fill available space entirely.

The transmission measurement will be conducted using different conditions mentioned above. We list Table 8.2 to summarize all the variable values in different conditions we used.

Table 8.2: Environment variables in our test

PDCCH Aggregation Level	1 / 2 / 4 / 8
Signal Attenuation from HeNodeB to UE (dB)	20 / 40

The PDCCH data from MeNodeB-1 in test conditions above will be received and analyzed at UE. The UE will decode the physical layer control channels (PCFICH, PHICH, PDCCH) in each DL subframe.

In order to obtain BER and BLER of PDCCH, UE will generate the DCI and code it into PDCCH locally for comparison with received one. SINR of received PDCCH complex-valued symbols will also be calculated. The comparison result recorded at UE will be post processed and analyzed offline.

In the single eNodeB scenario, same parameters are configured in the measurement as the heterogeneous network scenario did. All four different aggregation levels are used as well.

8.2 PDCCH in Single eNodeB Scenario

To one PDCCH, the uncoded DCI message bits are its actual payload. Physical layer PDCCH bits are derived from the DCI message bits. After CRC attaching, convolutional encoding and repetition coding, the uncoded DCI bits (including 16-bit CRC attachment) are size-expanded according to the chosen PDCCH aggregation level. The higher aggregation level corresponds to a higher coding rate, providing more robustness against interference and decoding error.

From macro-cell UE reception point of view, only a correctly recovered DCI message from PDCCH is useful, i.e. each DCI bit needs to be correctly decoded from a PDCCH and pass the Cyclic Redundancy Check (CRC). Despite the number of successfully recovered DCI bits, one bit decoding error in DCI will lead to failure of CRC check and subsequently lead to retransmission request of the whole PDCCH.

Hence, we will firstly use PDCCH block error rate (BLER) to measure the correctness of PDCCH reception and decoding at macro-cell UE. It is defined as the ratio of erroneous decoding PDCCH blocks to all received PDCCH blocks. Among all PDCCHs in each DL subframe, only one is configured for this UE and continuously allocated at the same position. The erroneously decoded PDCCH block is identified by conducting CRC check. Only having zero remainder of CRC check is a correctly received PDCCH.

We use average SINR of the received complex-valued QPSK symbols inside a PDCCH (E_s/N_o) to represent the channel condition during this PDCCH reception. The PDCCH BLER versus PDCCH symbols E_s/N_o will be presented for showing PDCCH capability of sustaining interference. Besides, we will also calculate the received PDCCH symbols SINR cumulative distribution function (CDF), to display the overall interference extent during the whole test.

On the other hand, only using PDCCH BLER will hide and omit some detail of how worse the PDCCH reception is interfered. One DCI bit error and more DCI bits error have the same effect of PDCCH decoding failure. Thus, we will also calculate the PDCCH payload (uncoded DCI bits) BER and give out its CDF as a supplement, in order to show how much the channel interference neutralizes the PDCCH coding gain.

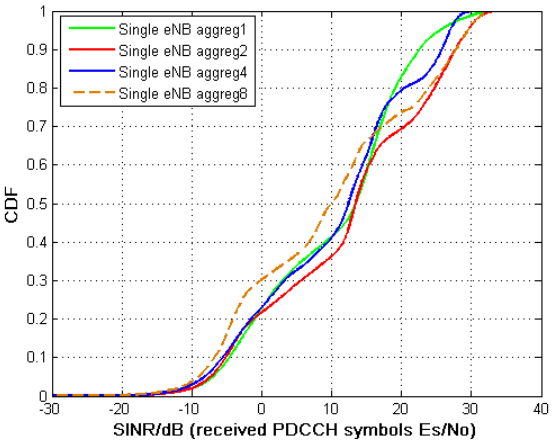

Figure 8.1: PDCCH symbol SINR (E_s/N_o) CDF (single eNodeB)

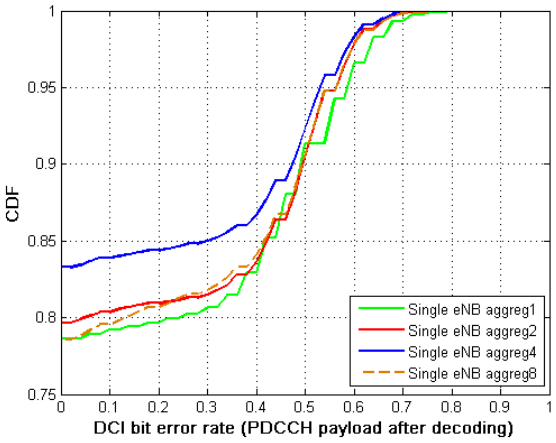

Figure 8.2: PDCCH payload (DCI bits) BER CDF (single eNodeB)

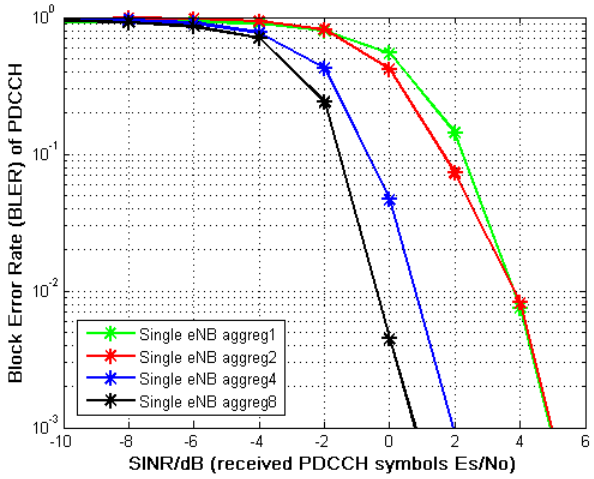

Figure 8.3: PDCCH BLER (single eNodeB)

In the single eNodeB transmission scenario, without external interference, four different aggregation levels have close PDCCH symbols SINR CDF curves, displayed in Figure 8.1. The different coding rates on these aggregation levels, however, provide different performance on PDCCH BLER, which is shown in Figure 8.3. Usually, no more than 1% BLER is required for PDCCH reception at UE. Apparently, the bigger aggregation level is used, the lower SINR is needed to fulfill such requirement. In our test set up, using aggregation 8 gives PDCCH close to a 4 dB advance than aggregation 1 to reach this goal.

When comes to PDCCH payload bits (uncoded DCI message bits) BER CDF result, which displayed in Figure 8.2, a strange situation can be witnessed. Among aggregation level 1, 2 and 4, the higher aggregation level has better BER CDF performance, which fits the

expectation since higher coding rate should have more robustness. However, DCI bits BER CDF of aggregation level 8 is worse than that of aggregation level 4 and stays close to those of aggregation level 1 and 2.

This phenomenon indicates some implementation loss may exist in our system, which makes the PDCCH loss some coding gain in some circumstances, especially when aggregation level 8 is used. It may impact the PDCCH BLER and BER measurement accuracy. For example, PDCCH BLER versus SINR curve of aggregation level 8 in Figure 8.3 could be even better (although it is already better than other aggregation levels).

8.3 Macro-cell PDCCH in Heterogeneous Network

Under co-channel deployment, the HeNodeB and the MeNodeB use same frequency band and run simultaneously in a heterogeneous network. As discussed in model implementation in Chapter 7.1, HeNodeB will actively coordinate its radio frame with MeNodeB-1. As a consequence, PDCCHs from two eNodeBs will overlap in the control region.

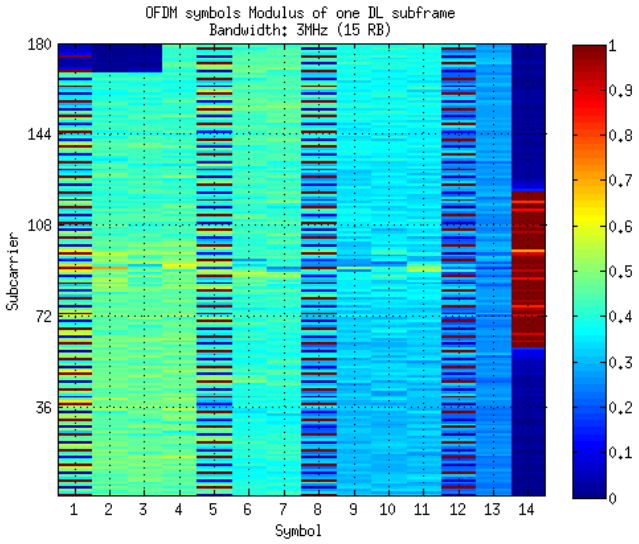

Figure 8.4: Spectrogram of overlapped DL subframe of HeNodeB and MeNodeB-1

The control region on DL subframe of MeNodeB-1 is configured to be fully loaded with the maximum possible number of PDCCHs while the HeNodeB's PDCCHs only use one third of the control region. The Figure 8.4 displayed the spectrogram of a DL radio subframe measured at UE, which is 14 symbols × 18 subcarriers in size. The color difference between regions presents the received symbols relative energy level. Areas with highest energy level

are synchronization symbols and cell specific reference symbols, which appear as dark red. We can spot that color in first several symbols of the subframe is relatively brighter than the rest of control region. It indicates PDCCHs of MeNodeB-1 and HeNodeB are overlapped there, leading to higher received symbol energy. Our target PDCCH (from macro-cell MeNodeB-1 to UE) is located inside the overlapping area.

The result of the heterogeneous network scenario will be compared with the single eNodeB transmission situation (the control group), for displaying the potential PDCCH performance degradation (on BLER, payload BER CDF and SINR CDF) brought by co-channel heterogeneous deployment.

As introduced in Chapter 7.2, at the heterogeneous scenario, the co-channel interference from HeNodeB to macro-cell UE will be attenuated by 20 dB and 40 dB respectively. The less attenuation, the more co-channel interference macro-cell UE will receive. The PDCCH BLER, PDCCH symbols SINR (E_s/N_o) CDF and DCI bits BER CDF under such two situations will be measured and compared to the single eNodeB scenario. This kind of comparison will be performed at each PDCCH aggregation level.

When using aggregation level 1, the results are displayed in Figure 8.5, Figure 8.6 and Figure 8.7.

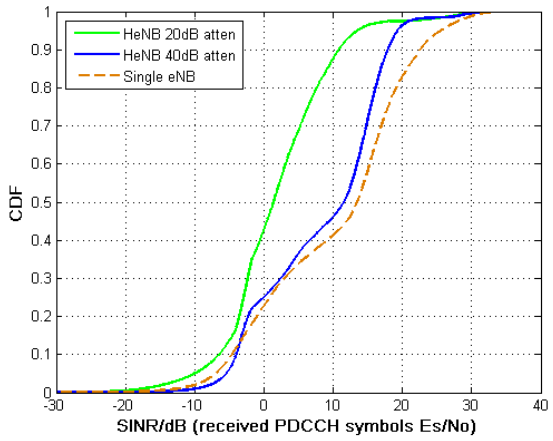

Figure 8.5: PDCCH symbol SINR (E_s/N_o) CDF (use PDCCH aggregation level 1)

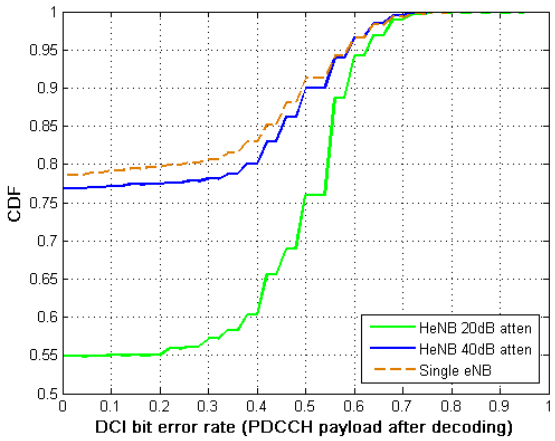

Figure 8.6: PDCCH payload (DCI bits) BER CDF (use PDCCH aggregation level 1)

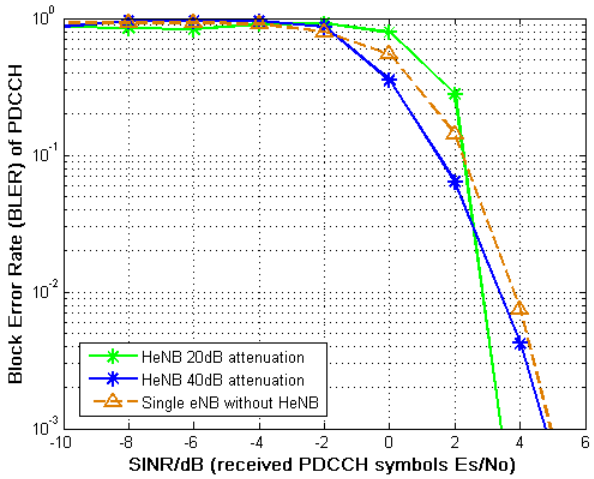

Figure 8.7: PDCCH BLER (use PDCCH aggregation level 1)

In the co-channel heterogeneous network, the macro-cell UE received PDCCH E_s/N_o CDF curves (in Figure 8.5) and PDCCH payload DCI message bits BER CDF curves (in Figure 8.6) are both deteriorated compared to single eNodeB scenario. The deterioration extent corresponds to co-channel interference strength.

On the other hand, the PDCCH BLER v.s. PDCCH E_s/N_o only shows a small difference between co-channel heterogeneous network and single eNodeB scenario (in Figure 8.7).

Next we test PDCCH aggregation level 2. The received PDCCH E_s/N_o CDF curves (in Figure 8.8) and the PDCCH payload DCI message bits BER CDF curves (in Figure 8.9) are still deteriorated compared to single eNodeB scenario. In addition, PDCCH payload BER CDF deterioration is corresponding to the co-channel intereference level from HeNodeB as well.

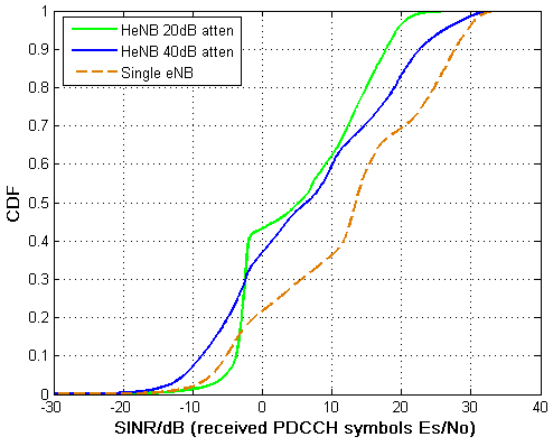

Figure 8.8: PDCCH symbol SINR (E_s/N_o) CDF (use PDCCH aggregation level 2)

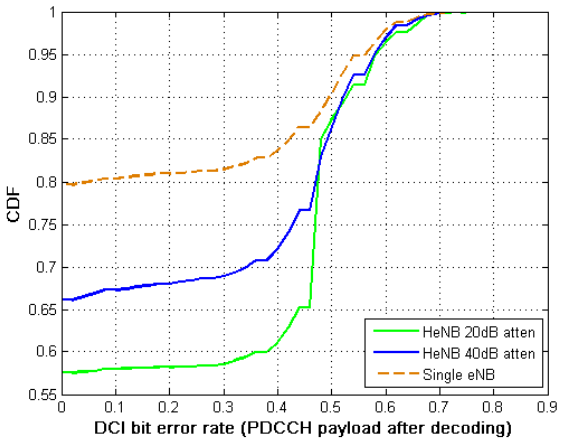

Figure 8.9: PDCCH payload (DCI bits) BER CDF (use PDCCH aggregation level 2)

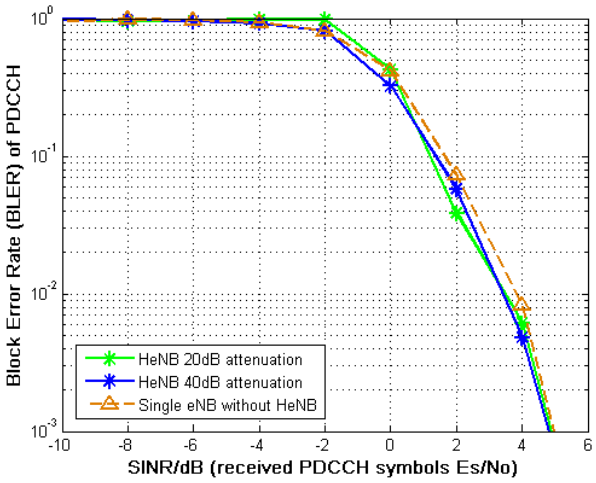

Figure 8.10: PDCCH BLER (use PDCCH aggregation level 2)

Presented in Figure 8.10, PDCCH BLER v.s. received PDCCH E_s/N_o has close performance in single eNodeB and heterogeneous deployment, same as the situation in aggregation level 1.

When using aggregation level 4, results are displayed below. Even though PDCCH symbols SINR CDF curves at two different inter-cell interfered conditions are very close to each other (but they are all worse than single eNodeB scenario), PDCCH payload BER CDF comparison performs similarly as that when aggregation level 1 or level 2 is used. Besides, PDCCH BLER comparison between single eNodeB scenario and two co-channel heterogeneous deployed situations still keep small disparity.

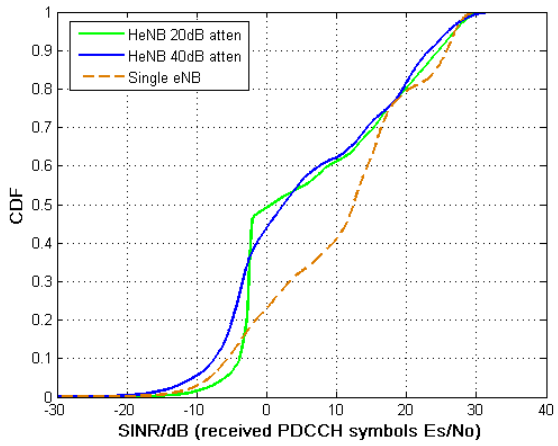

Figure 8.11: PDCCH symbol SINR (E_s/N_o) CDF (use PDCCH aggregation level 4)

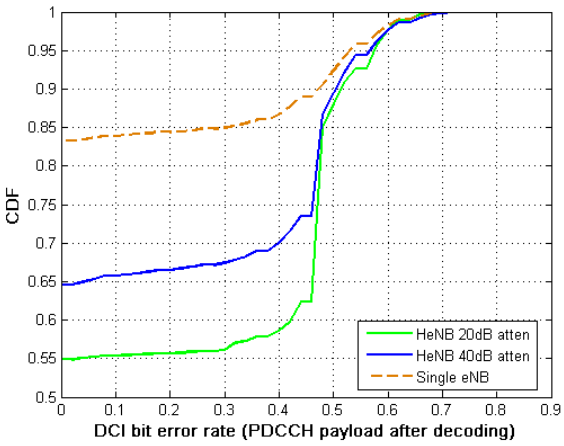

Figure 8.12: PDCCH payload (DCI bits) BER CDF (use PDCCH aggregation level 4)

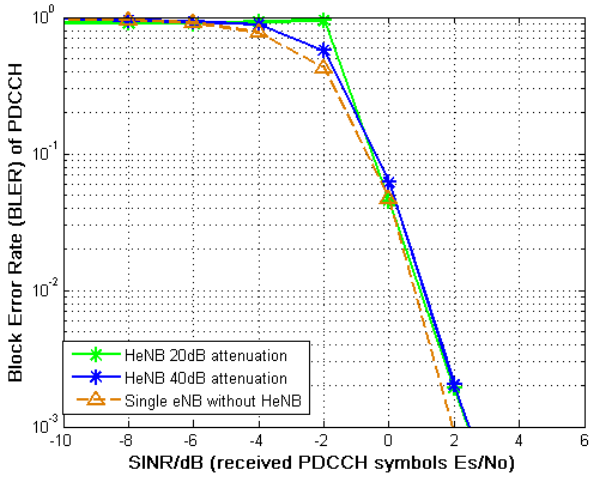

Figure 8.13: PDCCH BLER (use PDCCH aggregation level 4)

At last, we test with aggregation level 8. PDCCH symbols SINR CDF and PDCCH payload (DCI bits) BER CDF both reveal that co-channel heterogeneous deployment will deteriorate their performance compared to single eNodeB deployment, similar as those happen in other aggregation levels. However, unlike shown in other aggregation levels, PDCCH BLER v.s. SINR curves comparison at aggregation level 8 performs differently (in Figure 8.16). When HeNodeB to UE interference is attenuated by 20dB, macro-cell PDCCH BLER is degraded a lot (approximately 5 dB) in co-channel heterogeneous scenarios compared to the single eNodeB scenario. Such big degradation disappears when attenuation decreases to 40 dB where its PDCCH BLER is very close to the single eNodeB scenario.

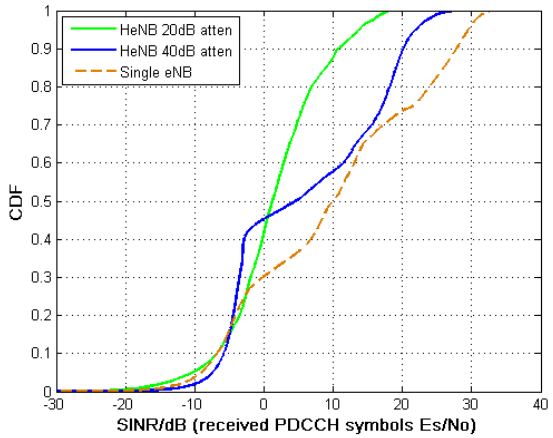

Figure 8.14: PDCCH symbol SINR (E_s/N_o) CDF (use PDCCH aggregation level 8)

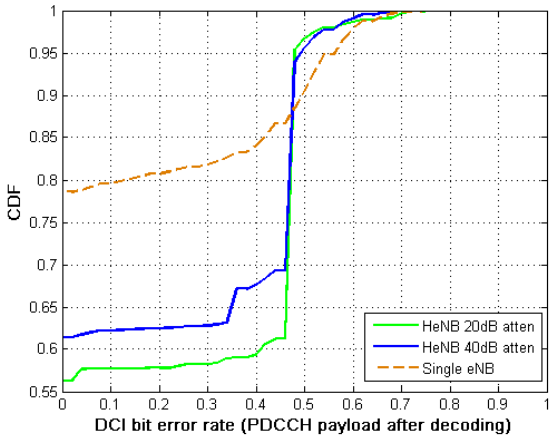

Figure 8.15: PDCCH payload (DCI bits) BER CDF (use PDCCH aggregation level 8)

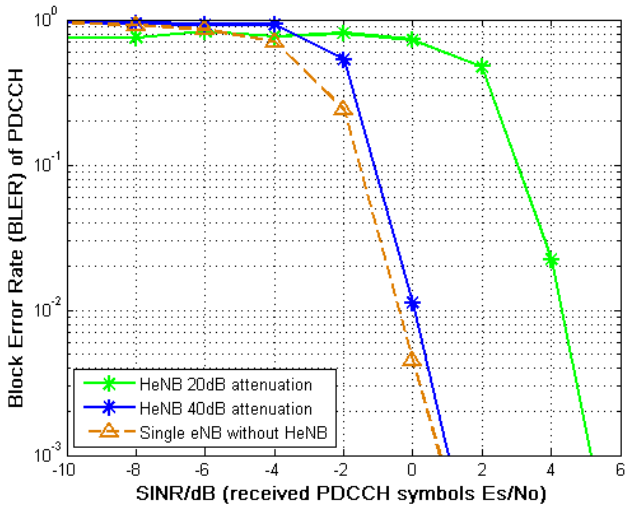

Figure 8.16: PDCCH BLER (use PDCCH aggregation level 8)

Overall speaking, the test results show that co-channel heterogeneous deployment degrades the macro-cell PDCCH performance to some extent. This deterioration is especially evident when expressed as PDCCH payload (DCI bits) BER CDF curves. The deterioration level of PDCCH payload BER CDF is always corresponding to the strength of co-channel interference from overlaid femto-cell HeNodeB. In addition, the received PDCCH symbols SINR (E_s/N_o) CDF is always worse in the co-channel heterogeneous network.

On the other hand, the PDCCH BLER in the co-channel heterogeneous network performs closely to the single eNodeB scenario. One of the reasons is that PDCCH coding gain compensates the reception error in some degree, which diminishes their BLER variation. One exception is when using aggregation level 8 where big difference on PDCCH BLER comparison is witnessed. The reason causes such an exception is currently unclear. However, we can point out some potential aspects that may contribute to it.

First, we have found some flaws exist in the system cause coding gain loss at PDCCH aggregation level 8, and potential on other aggregation levels as well which had been analyzed at the end of Chapter 8.2.

Besides, we had only tested with 20dB and 40dB attenuations respectively on the signal route from HeNodeB to UE. These attenuations may be too big to reveal the impact of co-channel interference to the PDCCH BLER, i.e. the PDCCH BLER may not be enough disturbed. The too weak co-channel interferences from HeNodeB have not provided big enough distinction to vary their corresponding BLER. The evidence is the PDCCH symbols E_s/N_o CDF curves comparisons within different heterogeneous interference intensities in the test. They, especially when PDCCH aggregation level 4 is used, are very close or only have a small disparity.

It will be interesting to check if configuring less attenuation, i.e. 10dB or 0dB, will the much stronger inter-cell interference deteriorate PDCCH BLER performance more and lead to evident difference compared to the single eNodeB situation.

At last, due to the software efficiency and limitation in the current system, the accuracy of the result may be disturbed. The Linux workstation that controlled the HeNodeB had a heavy calculation burden. Its functionality combines both eNodeB and UE. In each DL, it needs to work parallel on synchronizing received subframe from MeNodeB-1 like an ordinary UE, as well as preparing its own DL data like an ordinary eNodeB. The time alignment algorithm must be done fast enough to ensure transmitting DL at correct time slot. In our test, the software can only run less than one minute before crashing. Hence, the samples number we received was not very big. We also found that HeNodeB sometimes dropped several consecutive received subframes that would lead to the abandon of DL transmission in those subframes.

Research in [32] also reveals the shortcomings in such an SDR platform that runs on the general purpose processor with un-real-time operating system. They include packets loss in UDP communication between USRP and PC, frequency offset due to the USRP local oscillator inaccuracy, etc.

These problems will interfere the correctness of the test result.

8.4 Improvement on Test and Further Measurement

In this thesis, we built an SDR based test environment of heterogeneous LTE-TDD networks. We measured the macro-cell PDCCH performance when an overlapped femto-cell HeNodeB casted co-channel interference on it. In our test, we added 20dB and 40dB attenuations on HeNodeB output signal respectively. It revealed that PDCCH performance in the heterogeneous network would be deteriorated to some extent compared to the single eNodeB transmission scenario. When expressed as PDCCH payload BER CDF curves comparison, such deterioration is evident. When expressed as PDCCH BLER v.s. received PDCCH symbols SINR, the difference becomes very slight.

Based on shortage and problems analysis at the end of Chapter 8.3, in the future measurement we could test the configurations with 10dB and even 0dB attenuation levels on HeNodeB output. Check the macro-cell PDCCH performance under much stronger interference.

Besides, in the current test we enforce HeNodeB to coordinate radio frame timing with MeNodeB-1, or work in a “synchronous mode”. Even though it avoids the interference from femto and macro cells’ DL/UL subframes overlapping, it significantly increases HeNodeB

processing burden. Instead, we can adopt an “asynchronous working mode” at HeNodeB, letting it transmit at own pace and do not perform time alignment with macro-cell.

In the real environment, compared to the synchronous working mode, the asynchronous working mode will benefit the HeNodeB in heterogeneous network deployment. It will not need the backhaul signaling support nor the over the air sensing functionality for doing timing coordination. Hence, it can conspicuously decrease the system complexity and expense. It will be very interesting to compare the PDCCH performance between HeNodeB works in synchronous mode and asynchronous mode.

In order to measure the PDCCH performance in HeNodeB asynchronous mode, we have to configure asynchronous interference. Since radio frame overlapping situation is unpredictable, in order to test the worst case, we need to ensure macro-cell UE always receive interference from either femto-cell DL or femto-cell UL. Thus, we need to introduce PDSCH in HeNodeB DL transmission as well as UL PUSCH and PUCCH which will be transmitted by a new femto-cell UE.

This test scenario is proposed in Figure 8.17.

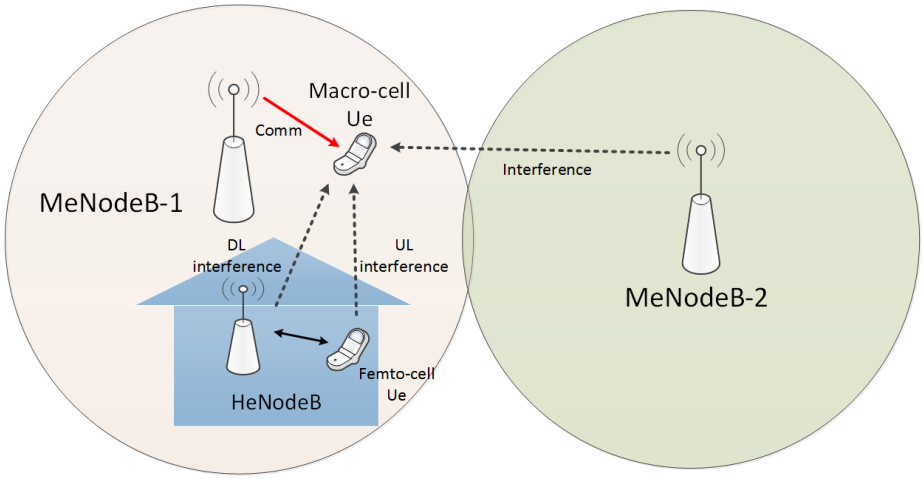

Figure 8.17: HeNodeB asynchronous working mode test scenario

Chapter 9

Conclusion

Femto-cell provides short-range cellular accessing service inside a building. It is easy to deploy, as it can be connected into an operator's core network via broadband cable in the building, without requiring sophisticated control signaling. It is an efficient supplement in indoor environments for providing coverage enhancement that conventional outdoor macro-cell networks cannot achieve, due to the penetration loss of building walls. In an LTE co-channel heterogeneous network, femto-cells that geographically locate inside a macro-cell, reuse the same frequency band as the macro-cell. The building penetration loss helps to alleviate the inter-cell interference. The spatial reuse of frequency provides enhanced capacity, compared to conventional way of spectrum partitioning between macro and femto cells. However, we still need to pay attention to inter-cell interference in co-channel transmission circumstance, in order to protect both macro-cell and femto-cell. Some special procedures like transmission power control [33] or cell identity number manipulation [19] can be adopted to mitigate the interference from femto-cell to macro-cell.

In this thesis, analysis of LTE-TDD heterogeneous network is focused on the interference on Physical Downlink Control Channel (PDCCH) brought by co-channel deployment. The ability of macro-cell PDCCH to sustain interference is evaluated by measurements on the test platform implemented during the thesis. PDCCH received Block Error Rate (BLER), PDCCH payload (DCI bits) BER and received PDCCH symbols SINR (E_s/N_o) are measured at macro-cell UE. We deploy software define radio devices (Ettus Research USRP 200 terminals) to work as eNodeB or UE, for simulating a co-channel heterogeneous environment. Linux workstations are connected to each USRP, running the baseband algorithms and processing software compiled from C++ code. Two macro-cell eNodeBs (MeNodeB), one femto-cell eNodeB (HeNodeB) as well as a macro-cell UE are set up. In the test, femto-cell HeNodeB is deployed to align its radio frame to macro-cell MeNodeB, i.e. synchronous mode.

Our test indicates that macro-cell PDCCH performance in a co-channel heterogeneous network will degrade to some extent compared to single eNodeB transmission scenario. The degradation mainly expresses in BER CDF of PDCCH payload (DCI message bits) and macro UE received PDCCH symbols E_s/N_o CDF. The PDCCH BLER, however, maintains similar performance compared to the single eNodeB scenario.

Based on the shortcoming of the current test set up, we also propose the improvement on the test. Furthermore, we introduce another femto-cell working mode under heterogeneous network for releasing HeNodeB calculation complexity, i.e. asynchronous mode. The PDCCH performance comparison between the synchronous and the asynchronous modes is also worth further investigation.

Reference

[1]. H. Shajaiah, A. Abdel-Hadi and C. Clancy, "Utility Proportional Fairness Resource Allocation with Carrier Aggregation in 4G-LTE," *IEEE Military Communications Conference (MILCOM)*, pp.412-417, Nov 2013.

[2]. J. Wannstrom, “Carrier Aggregation explained,” Jun 2013. [Online]: http://www.3gpp.org/technologies/keywords-acronyms/101-carrier-aggregation-explained.

[3]. A. Khandekar, N. Bhushan, T. Ji, and V. Vanghi, “LTE-Advanced: Heterogeneous networks,” *European Wireless Conference (EW),* pp. 978-982, Apr 2010.

[4]. V. Chandrasekhar, J.G. Andrews and A. Gatherer, "Femtocell networks: a survey," *IEEE Communications Magazine*, vol.46, no.9, pp.59-67, Sep 2008.

[5]. D. Tsolkas, N. Passas and L. Merakos, "Alleviating control channel interference in femto-overlaid LTE-advanced networks," *IEEE Communications Magazine*, vol.51, no.10, pp.192-200, Oct 2013.

[6]. Y. Wang, Y. Chang and D. Yang, "An Efficient Inter-Cell Interference Coordination Scheme in Heterogeneous Cellular Networks," *IEEE Vehicular Technology Conference (VTC Fall)*, pp.1-5, Sep 2012.

[7]. S. Rangan, “Femto-Macro Cellular Interference Control with Subband Scheduling and Interference Cancelation,” *IEEE GLOBECOM Workshops (GC Wkshps)*, pp.695-700, Dec 2010.

[8]. CISCO, “Cisco Universal Small Cell Solution: A Platform for Service Innovation,” *C22-733906-00*, Feb 2015. [Online]: http://www.cisco.com/c/dam/en/us/solutions/collateral/service-provider/small-cell-solutions/platform-for-service-innovation.pdf.

[9]. Small Cell Forum, “HeNB (LTE Femto) Network Architecture (Release 5),” *SCF025.05.01,* Dec 2013. [Online]: http://scf.io/en/documents/025_HeNB_LTE_Femto_network_architecture.php.

[10]. B. Li, "An Effective Inter-Cell Interference Coordination Scheme for Heterogeneous Network," *IEEE Vehicular Technology Conference (VTC Spring)*, pp.1-5, May 2011.

[11]. T. Yucek and H. Arslan, "A survey of spectrum sensing algorithms for cognitive radio applications," *IEEE Communications Surveys & Tutorials*, vol.11, no.1, pp.116-130, 2009.

[12]. G. Li, J. Fang, H. Tan and J. Li, "The impact of time-bandwidth product on the energy detection in the cognitive radio," *IEEE Broadband Network and Multimedia Technology Conference (IC-BNMT)*, pp.634-638, Oct 2010.

[13]. H. Tang, "Some physical layer issues of wide-band cognitive radio systems," *IEEE New Frontiers in Dynamic Spectrum Access Networks Symposium (DySPAN)*, pp.151-159, Nov 2005.

[14]. T. Yucek and H. Arslan, "Spectrum Characterization for Opportunistic Cognitive Radio Systems," *IEEE Military Communications Conference (MILCOM)*, pp.1-6, Oct 2006.

[15]. Z. Bharucha, G. Auer and T. Abe, "Downlink femto-to-macro control channel interference for LTE," *IEEE Wireless Communications and Networking Conference (WCNC)*, pp.1259-1264, Mar 2011.

[16]. CATT, "Analysis of Time-Partitioning Solution for Control Channel," *3GPP TSG RAN WG1 Meeting R1-103494*, Jun–Jul 2010.

[17]. Y. Wang and K.I. Pedersen, "Performance Analysis of Enhanced Inter-Cell Interference Coordination in LTE-Advanced Heterogeneous Networks," *IEEE Vehicular Technology Conference (VTC Spring)*, pp.1-5, May 2012.

[18]. 3GPP, "Evolved Universal Terrestrial Radio Access (E-UTRA); FDD Home eNodeB (HeNB) Radio Frequency (RF) Requirements Analysis (Release 9)," *TS 36.921 v9.0.0,* Mar 2010.

[19]. Z. Bharucha, G. Auer, T. Abe and N. Miki, "Femto-to-Macro Control Channel Interference Mitigation via Cell ID Manipulation in LTE," *IEEE Vehicular Technology Conference (VTC Fall)*, pp.1-6, Sep 2011.

[20]. S. Sesia, I. Toufik and M. Baker, "LTE - The UMTS Long Term Evolution: From Theory to Practice," 2nd ed, John Wiley & Sons, 2011.

[21]. 3GPP, "3rd generation partnership project; Technical specification group radio access network; Physical Channels and Modulation (Release 8)," *TS 36.211 v8.9.0,* Dec 2009.

[22]. R. Ratasuk, A. Ghosh, W. Xiao, R. Love, R. Nory and B. Classon, "TDD design for UMTS Long-Term Evolution," *IEEE Personal, Indoor and Mobile Radio Communications Symposium (PIMRC)*, pp.1-5, Sep 2008.

[23]. M. Rinne and O. Tirkkonen, "LTE, the radio technology path towards 4G," *Computer Communications*, vol.33, no.16, pp.1894-1906, Oct 2010.

[24]. J. Brown and J.Y. Khan, "Performance comparison of LTE FDD and TDD based Smart Grid communications networks for uplink biased traffic," *IEEE Smart Grid Communications Conference (SmartGridComm),* pp.276-281, Nov 2012.

[25]. E. Lähetkangas, K. Pajukoski, J. Vihriälä, G. Berardinelli, M. Lauridsen, E. Tiirola and P. Mogensen, "Achieving low latency and energy consumption by 5G TDD mode optimization," *IEEE Communications Workshops (ICC),* pp.1-6, Jun 2014.

[26]. D. Poulin, "FDD vs TDD Comparison," Oct 2013. [Online]: http://www.slideshare. net/darcypoulin/tdd-versus-fdd.

[27]. H. Holma and A. Toskala, "LTE for UMTS: OFDMA and SCFDMA Based Radio Access," 1st ed, John Wiley & Sons, 2009.

[28]. 3GPP, "3rd generation partnership project; Technical specification. LTE; Evolved Universal Terrestrial Radio Access (E-UTRA); User Equipment (UE) radio transmission and reception (Release 8)," *TS 36.101 v8.25.0,* Sep 2014.

[29]. 3GPP, "3rd generation partnership project; Technical specification group radio access network; Multiplexing and Channel Coding (Release 8)," *TS 36.212 v8.8.0*, Dec 2009.

[30]. 3GPP, "3rd generation partnership project; Technical specification group radio access network; Physical Layer Procedures (Release 8)," *TS 36.213 v8.8.0*, Sep 2009.

[31]. P. Amin, O. Tirkkonen, T. Henttonen and E. Pernila, "Primary component carrier selection for a heterogeneous network: A comparison of Selfish, Altruistic and Symmetric Strategies," *IEEE Wireless Communications and Networking Conference Workshops (WCNCW),* pp.115-119, Apr 2012.

[32]. J. Kerttula , N. Malm , K. Ruttik , R. Jäntti and O. Tirkkonen, "Implementing TD-LTE as software defined radio in general purpose processor," *ACM Workshop on Software Radio Implementation Forum*, pp.61-68, Aug 2014.

[33]. X. Li, L. Qian and D. Kataria, "Downlink power control in co-channel macrocell femtocell overlay," *Information Sciences and Systems Conference (CISS)*, pp.383-388, Mar 2009.